Pumpless Open-Surface Microfluidic Device for Protein Detection

BY

HELENE DELLA MONICA
B.S., Politecnico di Torino, Turin, Italy, 2017

THESIS

Submitted as partial fulfillment of the requirements
for the degree of Master of Science in Mechanical Engineering
in the Graduate College of the
University of Illinois at Chicago, 2019

Chicago, Illinois

Defense Committee:

Prof. Constantine M. Megaridis, Chair and Advisor
Prof. David Eddington, Bioengineering
Prof. Pietro Asinari, Politecnico di Torino

Alla mia Famiglia, la mia fonte di sostegno e felicità

ACKNOWLEDGMENTS

Firstly, I would like to express my sincere gratitude to my advisor Prof. Constantine Megaridis for the continuous support during my Master thesis, for his patience and motivation. His guidance helped me in all the time of research and writing of this thesis. Besides my advisor, I would like to thank the rest of my thesis committee: Prof. David Eddington, who provided me an opportunity to join his laboratory, and Prof. Pietro Asinari for his insightful comments and encouragement. I thank my fellow labmates for the stimulating discussions and for all the fun we have had in the last months. In particular, my sincere thanks goes to Jared and Maheshwar. Without their precious support it would not be possible to conduct this research.

Thanks to my roommates Lorenzo and Claudia, who made our house a peaceful and fun place where I felt at home. Thanks all my friends Vale, Betta, Tuzza, Elly, Alina, and Ceci for being closed to me even far from home. A very special word of thanks for Borghets, who teaches me that a strong friendship can grow even in few years with trust and understanding. Thanks for always being for me. I would also like to thank Gasty, who shared with me one of my greatest passions, ballet,a source of happiness after the days at Politecnico di Torino.

A special thanks to Jacopo, who encouraged me throughout this experience and supported me in my everyday life. During these years, he pushed me to achieve my greatest potential. I find myself lucky to have a person like him in my life.

Finally, my heartfelt thanks to all my family. They provided me with the opportunity to be where I am today, standing behind me with their love and support. Thank you to my father, my

point of reference, for always looking out for my future and conveying the value of hard work, perseverance and love for others. Thanks to my mother, who taught me how to take life lightly and always with the smile, and to my brother Pio, who is always beside me with his hidden and silent gestures.

HDM

TABLE OF CONTENTS

LIST OF TABLES

LIST OF FIGURES

LIST OF FIGURES (continued)

FIGURE **PAGE**

LIST OF FIGURES (continued)

LIST OF FIGURES (continued)

LIST OF FIGURES (continued)

FIGURE **PAGE**

LIST OF ABBREVIATIONS

APTES	3-aminopropyltriethoxysilane
BCA	Bicinchoninic acid assay
BSA	Bovine serum albumin
CA	Contact Angle
DIW	Deionized water
EDC	1-ethyl-3-[3-dimethylaminopropyl]carbodiimide hydrochloride
ELISA	Enzyme-linked immunosorbent assay
EWOD	Electrowetting on dialetric
KOH	Potassium hydroxide
LOC	Lab-on-chip
PBS	Phospate/buffered saline
POC	Point-of-care
S	Spreading parameter
SNHS	N-hydroxysulfosuccinimide
U	Cohesion energy of molecule into liquid
γ	Surface Tension

LIST OF ABBREVIATIONS (continued)

k^{-1}	Capillarity length
ρ	Density

SUMMARY

The present work focuses on the development of an open-air, passive microfluidic device to be employed for the detection of antigens, with the ultimate goal of performing the analysis and quantification of proteins contained within human skin oil. In the prototyping step, bovine serum albumin proteins (BSA) are detected by implementing a bicinchoninic acid (BCA) assay. The design of the device allows pumpless transport of a solution, made of BSA and DI water, and the coverage of a detection zone. The latter zone is silane-functionalized, so that proteins can be immobilized on its surface. Different wettability-patterned designs are considered and tested. Ultimately, the optimal design is composed of an axial, silane-functionalized track located between two superhydrophilic transport tracks, where the three tracks are patterned on a superhydrophobic background. The geometry (*e.g.* wedge angles) of the detection and transport tracks is optimized in order to obtain the largest covered detection area, with the lowest possible sample volume. Subsequently, BCA detection is performed on the substrate characterized by the aforementioned design and a standard curve is obtained by analyzing samples with a known concentration of proteins.

CHAPTER 1

INTRODUCTION

1.1 Capillarity and Wettability Patterning

A liquid could be imagined as a stretched elastic membrane characterized by surface tension that opposes its distortion.

From the microscopic point of view, a liquid is characterized by molecules that attract each other. In the midst of the liquid, a molecule is in a condition in which it interacts with all its neighbors. On the other hand, a molecule on the surface of the liquid loses half of such interactions. That means that if the cohesion energy of a molecule into the liquid is U, a molecule on the surface has an energy equal to U/2. For that reason, the liquid adjusts its shape in order to expose the smallest possible surface area to the external environment (Figure 1).

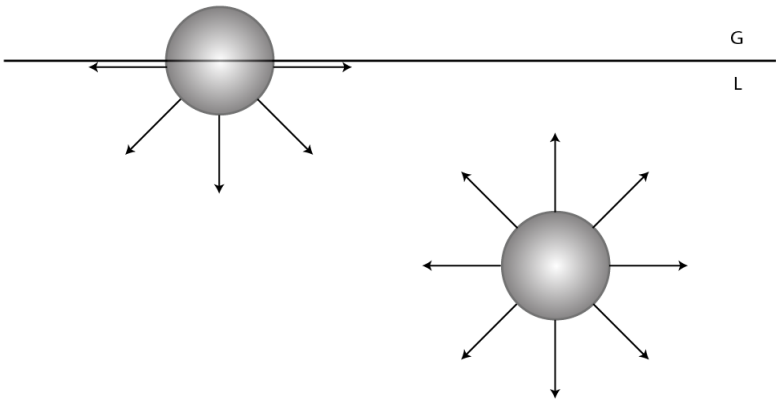

Figure 1: Molecules at the surface experience half of the attractive interactions, while molecules within the liquid benefit from interactions with their neighbors. The horizontal line represents the interface between liquid and gas.

The surface energy or surface tension, generally indicated with the symbol γ, is a measure of the cohesion energy per unit of area. If the dimension of the molecule is a and the surface area is a^2, the surface energy is approximately:

$$\gamma \simeq \frac{U}{2a^2} \tag{1.1}$$

Dimensionally, the surface energy is expressed in units as $\frac{mJ}{m^2}$ or $\frac{mN}{m}$ and it is defined as "the energy that must be supplied to increase the surface area by one unit" [1].

All liquids have a surface tension and each surface is characterized by a surface energy. By considering these two factors, it is possible to determine the behavior of a droplet that is in contact with a solid. Two main types of wetting regimes exist and are represented in Figure 2. The spreading parameter (S) describes these regimes and is defined as the difference between the surface energy of the wet and dry substrate:

$$S = E_{dry} - E_{wet} \tag{1.2}$$

$$S = \gamma_{SG} - (\gamma_{SL} + \gamma_{LG})$$

where the three surface tensions represent the solid/air γ_{SG}, solid/liquid γ_{SL} and liquid/air γ_{LG} interfaces.

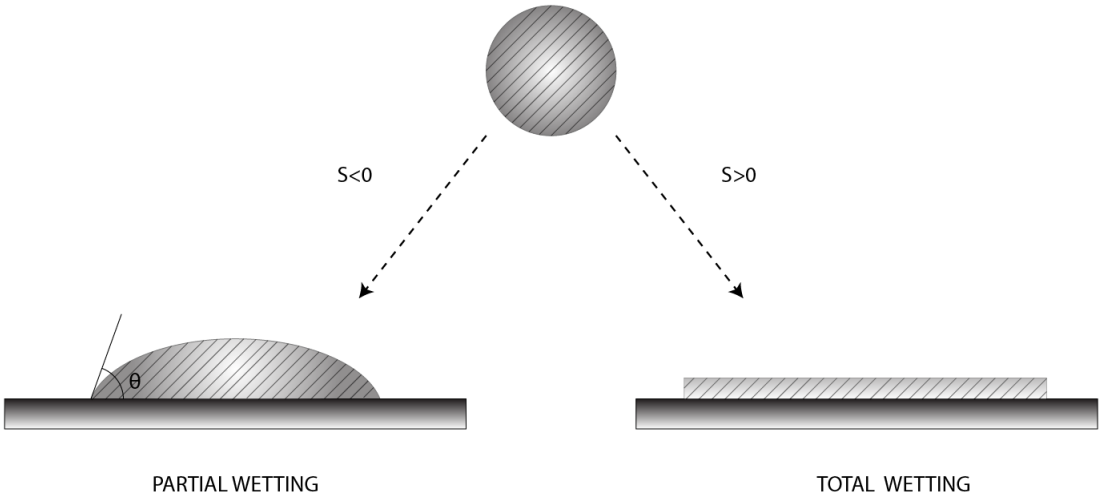

Figure 2: Two wetting regimes for a liquid droplet according to the spreading parameter S: partial wetting ($S < 0$) and total wetting ($S > 0$). θ is the angle between the surface and the tangent to the liquid droplet (also known as contact angle CA) at the contact line.

The spreading parameter S identifies two regimes:

- Total wetting $S > 0$: It is the condition in which a droplet of liquid completely spreads on the surface in order to reduce its surface energy (contact angle $\theta_E = 0$, angle the liquid makes with the surface). A film of fluid with a thickness of the order of nanometers is formed, which results from a balance between the molecular and the capillarity force.

- Partial wetting $S < 0$: the condition in which a droplet of liquid does not spread on the surface , but a spherical cap is formed on the surface with a contact angle θ_E. A liquid is called “mostly wetting", if the contact angle is $\theta_E \leq \frac{\pi}{2}$, and "mostly non-wetting", if the contact angle is $\theta_E \geq \frac{\pi}{2}$. Similarly, a surface is called "hydrophilic", if the contact angle of the liquid is $\theta_E \leq \frac{\pi}{2}$, and "hydrophobic", if the contact angle of the liquid is $\theta_E \geq \frac{\pi}{2}$. Moreover, if the contact angle $\theta_E \geq 150°$, the surface is defined to be superhydrophobic (droplets that touch superhydrophobic surfaces will bead up). If the contact angle is $\theta_E \leq 5°$ the surface is defined as being superhydrophilic (droplets that touch superhydrophilic surfaces will spread out completely).

The condition $\theta_E = \frac{\pi}{2}$ does not play an important role from the equilibrium transition state. The condition of hydrophilic and hydrophobic surface is showed in Figure 3.

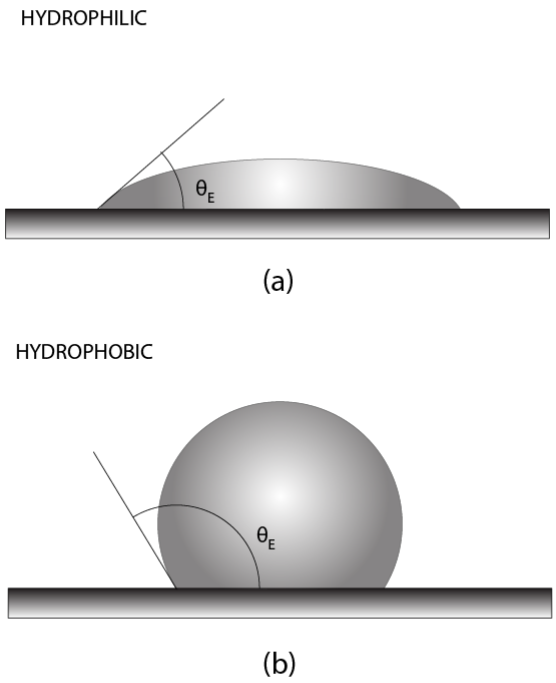

Figure 3: Schematic of a droplet deposited onto (a) hydrophilic surface ($\theta_E \leq 90°$) and (b) hydrophobic surface ($\theta_E \geq 90°$).

Contact angles CA can be measured by two main methods (Figure 4):

1. The first way is to consider a force balance. In particular, the sum of capillary forces that are acting on the line of contact at equilibrium has to be equal to 0. By normalizing the force per unit of length $[\frac{N}{m}]$, these force are the surface tensions between the three phases

(Solid,liquid and gas). By computing the equilibrium of the forces along the solid plane (x direction), we derive the famous Young's relation:

$$\gamma_{LG} cos\theta_E = \gamma_{SG} - \gamma_{SL} \tag{1.3}$$

Substituting the equation 1.1 in the above relation, yields:

$$S = \gamma_{LG}(cos\theta_E - 1) \tag{1.4}$$

The angle θ_E is defined only if the spreading parameter is negative. Moreover, it is evident that this angle increases as the liquid is non-wetting. For what concern the equilibrium of the forces along the vertical direction, the capillary forces are balanced by the reaction force exerted by the solid surface.

2. The second method relies on computing the work done to move the contact line over a certain distance dx. At equilibrium, this work is equal to zero:

$$\delta W = (\gamma_{SG} - \gamma_{SL})dx - \gamma_{LG} cos\theta_E dx \tag{1.5}$$

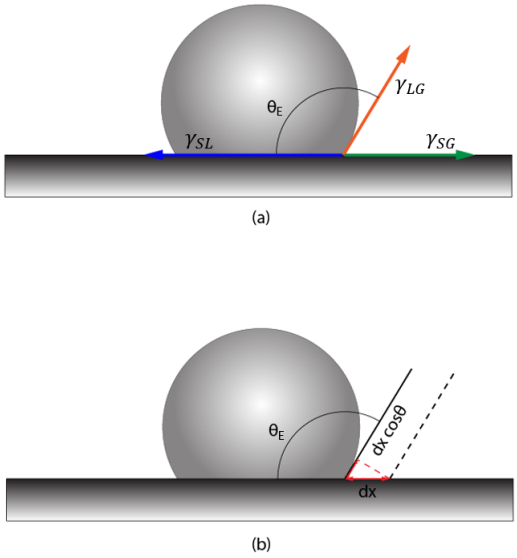

Figure 4: Determination of contact angle θ_E: (a) via forces (Young's relation) or (b) via work.

The two main factors that distinguish a superhydrophobic from a superhydrophilic surface are: the surface chemistry and surface roughness. The surface chemistry determines whether the surface has low or high surface energy, which determines whether the surface is hydrophobic or hydrophilic. Generally speaking, surfaces with low surface energy are hydrophobic, while surfaces with high surface energy are hydrophilic. In regards to surface roughness, surface texture usually makes hydrophobic surface even more hydrophobic (superhydrophobic) and an hydrophilic surface even more hydrophilic (superhydrophilic). A liquid droplet in contact with a rough surface exhibits two different behaviours which can be described by two models. In order to analyze them, it is necessary to define two parameters: the equilibrium contact angle

θ_E, which is for an ideal flat surface (given by Young's relation) and the apparent contact angle θ^* , which is for a rough surface.

These two models were developed by Cassie-Baxter and Wenzel and they show how surface roughness can affect a droplet contact angle. In Wenzel's model, it is assumed that the roughness scale is much smaller with respect to the size of the drop and the surface is homogeneous. The surface roughness is quantified by R, defined as follow:

$$R = \frac{\text{Real surface area}}{\text{Projected surface area}} \tag{1.6}$$

Since every surface has some sort of roughness, because no surface is no completely smooth at the molecular level, it is possible to assume that $R \geq 1$. Wenzle's model states:

$$cos\theta^* = Rcos\theta_E$$

Since $R \geq 1$, $|cos\theta^*| \geq |cos\theta_E|$

In fact, when θ_E is less than 90°, $\theta^* \leq \theta_E$. On the contrary, when θ_E is greater than 90°, $\theta^* \leq \theta_E$. Hence, this equation shows that roughness will make a hydrophobic surface even more hydrophobic and a hydrophilic surface even more hydrophilic. Thus, the effect of the surface roughness is always to magnify the wetting properties of a surface.

In Cassie Baxter's model, it is assumed that the surface is planar, chemically heterogenous and made of two species, each defined respectively by a characteristic contact angle θ_1 and θ_2. Moreover, it is assumed that these individual areas are much smaller with respect to size of the droplet. By defining f_1 and f_2, the fractional surfaces areas of the two species, Cassie Baxter states:

$$cos\theta^* = f_1 cos\theta_1 + f_2 cos\theta_2 \tag{1.7}$$

However, by considering the case of an hydrophilic surface ($\theta_E < 90°$) and an hydrophobic surface ($\theta_E > 90°$), Wenzel's model presents some critical aspect.

On a very rough hydrophilic surface, liquid penetrates the grooves of the surface and there are no air bubbles underneath the droplet, which is in complete contact with the surface. It is supposed that the grooves are completely filled with the liquid and the elevated surface is dry (partial wetting regime) Figure 5. By defining Φ_S the percentage of solid in contact with the liquid, it is possible to compute the apparent contact angle θ^* of the mixed surface with Cassie-Baxter relation Equation 1.7, by considering the contact angles of the individual species θ_E and 0:

$$cos\theta^* = -1 - \Phi_S + \Phi_S cos\theta_E \tag{1.8}$$

Since $\theta_E > 0$ (partial wetting regime), that implies θ^*=0 (total wetting), which is a condition not predicted by Wenzel‘s model.

On the contrary, for hydrophobic rough surfaces, since the surface tension of the dry substrate is lower than the wet one, the liquid is unlikely to fill the grooves of the solid surface. Therefore, the droplet sits on the top of tiny air bubbles that are in the pores of the solid substrate. As previously, by defining Φ_S as the percentage of solid in contact with the droplet and the equilibrium contact angle θ_E given by Young‘s relation, the apparent contact angle θ^* can be computed as:

$$cos\theta^* = -1 + \Phi_S(cos\theta_E + 1) \tag{1.9}$$

Hence, for the hydrophobic surface, $cos\theta^* \leq \Phi_S - 1$ and approaches π when the percentage of solid in contact with the droplet approaches zero.

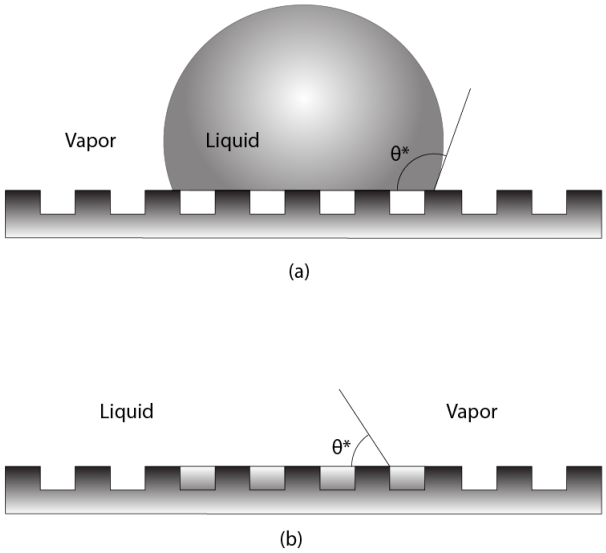

Figure 5: (a) Hydrophobic surface where the liquid does not fill the grooves of the surface and (b) hydrophilic surface, where the liquid fills spontaneously the grooves of the surface.

1.2 Point-of-care and Lab-on-chip Devices

Microfluidics is the science that controls and manipulates limited volumes of fluids (ranges from milliliters to picoliters) in channels or tracks of small dimensions, varying from millimeters (10^{-3}) to micrometers (10^{-6}). Since the 1980s, microfluidics has become of considerable interest in many science fields for achieving different microdroplet handling tasks (e.g. metering, transport, dispersing, separation, mixing) with a multitude of advantages [2]. The technology that achieved resounding successes in the recent years is the "Lab-on-chip" system (also known

as LOC), an approach in which a diagnostic laboratory is scaled it down into a very small chip. The key words that best describe this approach are miniaturization and integration. In fact, laboratory assays could be integrated directly in a small microfluidic system, on which it is possible to develop an entire laboratory protocol for a given experiment by performing multiplexing analysis.

There are potential advantages associated with LOC systems [3]. First of all, microfluidic devices for some aspects tend to be cheaper with respect to the conventional macro-scale machines. In fact, the miniaturized components require little energy for the proper functioning of the device, representing a high saving from the economic point of view. In some cases, it is not necessary to have external energy components and this enables to perform handling fluid tasks at zero cost. Another aspect that allows cost cutting is the lower consumption of reagents and chemicals, especially when they are very expensive. In fact, the Lab-on-chip systems offer significant possibility to reduce the volume of samples and reagents needed to perform the analysis. Furthermore, microfluidic devices have gained great importance for their quick processing and rapid response that leads to an enhancement of efficiency and reliability of analytical results. In addition, the reduced size ensures the portability of the device and a much shorter operating time.

The main applications of microfluidic devices are summarized in the following points:

- Chemistry (microreactors)

- Cosmetics (eye Irritation Tests of Cosmetics)
- Energy (microfuel technology)
- Biology (biosensor for enzymatic or DNA analysis)
- Health (point-of-care diagnostic device)
- Pharmaceuticals (drug delivery)

To interpreter the test results of all above applications, a chemical analysis usually has to be performed. Before the introduction of the LOC devices, chemical analysis has been typically performed in central laboratory where a trained and specialized personnel and specific equipment are required. The research objective is to make the chemical analysis feasible for a user that does not have experience and knowledge on this practice. Some examples that highlights this goal are the blood glucose concentration test for diabetic people or pregnancy tests. In both cases, the lab-on-chip is seen as a black box where the individual has only to push a button to start the analysis and after some minutes could retrieve the results which are easy to interpret. The test can be performed directly at home without a special training in chemistry by the user. These devices are widespread nowadays on the market, because they are efficient and economic.

Lab-on-chip has also gained great importance in immunoassay applications to detect viruses, bacteria and cancers based on antigen-antibody reactions [4]. The development of this technology in the medical research field plays an important role in the improvement of the global health, especially in countries in which there are few health care laboratories and resources,

and where diseases and infections are widespread. In some cases, there is availability of drugs to treat some specific diseases or illness, but there is a lack of diagnostic systems to identify patients that need that cure. Nowadays, the goal of the researchers is to create Point-of-care devices (particular lab-on-chip devices that can be adopted directly by the patient to monitor health) without laboratory support. An example (2010) is the study of a way to diagnose and manipulate the HIV infections [5]. Ten years ago, around 40 million people were affected with HIV in the world and only 1.3 million of them were accessing antiretroviral therapy. Around 90% of people infected with HIV did not know their HIV status. By measuring the quantities of CD4+ lymphocytes in the blood it is possible to determine if a person has HIV and follow the progress of their infection. The diagnostic tool to measure CD4 required complex technologies and the submission of the results to a central laboratory (requiring long time for retrieving the outcome). These techniques were not available in most of the developing countries because they required expensive equipment and trained technicians. However, with the introduction of Point-of-care HIV diagnostic, these issues are overcome.

Despite the many advantages of LOC devices and their utility, the combination of the expense and the complexity preclude their extensive adoption [6]. In fact, these devices are not widely available because most of the systems fail to be translated into a physical product due to complicated manufacturing procedures. Other critical issues are the lack of standards materials, the sample and process development. One common technique for the production of microfluidic device is lithography. This approach of manufacturing poses obstacles for the producers and the

users. Where high requirements are needed, such as clean rooms and silicon processing, manufacturing requires many steps and different tools and chemicals. Thus, there is the ongoing need to reduce the barriers in order to obtain a device simply-made and easy to purchase. Recently, paper-based microfluidics has shown great promise in decreasing the cost and increasing the simplicity of the device fabrication [7]. The development of these new technologies enhanced access to microfluidics, but it is not possible to produce devices with the same complexity of those systems produced with lithography or other 3D printing processes. But complex is not always analogous to being functional and efficient. Often, with simple fabrication protocols, it is possible to translate a digital design into real simple-to-use and easy-to-operate system. Paper based microfluidics are an excellent solution to satisfy these requirements.

The microfluidic systems are essentially divided in two main categories: Closed-channel and open-channel [8]. The first class is the most conventional system adopted and available on the market. These devices are characterized by an arrangement of microchannels where the fluid needs to be bounded between solid channel walls. In a open-channel device, the fluid flows on a free-surface, that means that it is not confined in channels or micropipings. The present study is focused on a specific open-surface device that employes wettability patterning to generate superhydrophilic wedge-shaped tracks on top of a superhydrophobic background. This contrast between the two domains is utilized as confinement for the droplets of liquid. In that way, the fluid can move along the axial direction of the track driven by the capillarity force. The aim of the work is to apply this system to the biomedical field for the diagnostic analysis of

multiple properties of particular biological fluids. Since the device analyzed in this work is an open-surface device, more details about this type of technology are provided in the next section.

1.3 Open-Air Devices

Open-channel or open-surface devices are recently-developed systems that deal with the transport of microvolumes of fluid without requiring bonding [9]. Thus, the fluid is not completely confined in microchannels, but it is exposed directly to the surroundings (air or other media). This can be obtained by creating well-defined ways to confine the fluids. Open-channel devices are usually adopted to overcome the issues of closed-channel devices. In fact, thanks to these devices it is possible to solve the problem of debris that lead to fouling [10], the passage of air-bubbles (multiphase fluid) that could clog channels [11] and the possible absorption of reagents on the surface of the channel walls. Moreover, the time necessary to produce and fabricate them is one order of magnitude shorter compared to the closed-channel systems [12]. In addition, fabricating open systems does not require complex and expensive manufacturing procedures. For that reason, open microfluidics are low-cost devices. In fact, the costs are reduced for the absence of microchannels and for the possibility to adopted simple and accessible materials, such as paper or plastic. Furthermore, open microfluidic devices possess high adaptability and accessibility because it is possible to manipulate and observe the fluid during the experiment at every point along the track, by adding or removing reagents.

Open-surface devices can be *Active* or *Passive*, depending on the presence of external energy input. Active open-surface devices are usually complex because they are characterized by external components (*e.g.* micropumps, syringes, microvalves, micromixers). This complexity and the need of the external power contribute to higher costs. There are different applications for active microfluidics devices: electrowetting on dialetric (EWOD), magnetic, dialectrophoretic, acoustic method (SAW), thermocapillary actuation. These technologies tend to be very effective, but the implementation could be complex and costly. In order to limit the development of these energy consuming platforms and to avoid onerous fabrication, passive microfluidic devices have been promoted. These systems are simple, effective, cheap and rapid. They are characterized by pumpless transport (without need of dedicated components), in which the force responsible for the movement of the fluid is the capillary force.

There are different techniques that have gained great deal of interest in recent years, which have the goal to pumplessly transport liquid droplets by inducing a spatial gradient of wettability at the surface. The micropatterning [13] and the physical texturing [14] is a procedure that takes advantage from the non-uniform roughness of the substrate to induce the flow of the fluid. Another technique is to produce a surface energy gradient. This may be achieved by a chemical modification of the droplets [15] or of the substrate [16], either by differential heating [17], photo irradiation [18] or by thermocapillary migration [19]. All these procedures permit the control and the manipulation of droplets within open-channel devices without electrical, pneumatic, or mechanical actuation systems. This work focused on a passive open-surface device that high-

lights all advantages of this category: simple, small, cheap and effective.

1.4 Pumpless Fluid Transport on Open Platforms

The transport of a liquid droplet on an open platform, driven only by the capillary force and without the need of other power inputs, has gained great importance in the recent years, especially in the biomedical field for the fabrication of low-cost diagnostic devices. Groups of researchers have studied that different techniques to achieve the passive transport of liquid droplets exist, which consist generally in altering the chemical pattern [20] or the physical texture of the surface [21]. A study regarding a wettability patterning for pumpless fluid transport has been conducted by Ghosh et al. [22], who produced superhydrophilic tracks that are capable of inducing a controlled on-chip movement of liquid droplets with have a characteristic dimension comparable to the capillarity length, by overtaking viscous and other opposing force, such as gravity, achieving high velocities ($\sim 400\ mms^{-1}$). Furthermore, this design is capable of transporting liquid volume ranging from 1 μl to 500 μl (cumulative transport due to a repeated disposal of multiple small liquid droplets).

The droplet, which has a size considerably larger (~ 2 mm) than the narrowest track edge ($\sim 550\ \mu$m) on which it is deposited, is constricted by the boundaries of the wedge shape track to move along the transverse direction(Figure 6). In fact, it is possible to observe an advancing film of fluid that proceeds towards the wider edge of the track to reduce the surface energy along this direction. The initial propagation of the liquid droplet is due to hemiwicking [22],

that consists in the spreading of the liquid on a rough superhydrophilic surface driven by an unbalanced capillary force along the track. Thus, when the liquid front spreads along the wedge-shaped track, the initial liquid bulge gradually disappears and a conical rivulet-shaped is formed.

Prior studies on this behavior was noticed by other researchers, who demonstrated that the shape of the liquid accumulated on superhydrophilic rectangular tracks patterned on a superhydrophobic background depends the ratio $\frac{\Omega}{\delta^3}$, where Ω represents the volume of the liquid and δ the width of the track [23]. When the value of this ratio is below a critical value that is determined by the equilibrium of the contact angles on the superhydrophilic and superhydrophobic domains, a semi-cylindrical shape is assumed by the liquid.

The liquid motion is influenced by the difference in the Laplace pressure between the front and the back of the bulge. The local Laplace pressure at each section of the liquid is defined as $\sim \frac{\gamma_{LG}}{r(x)}$, where r(x) represents the curvature of the liquid $r(x) \approx \frac{\delta(x)}{2sin\theta(x)}$. Thus, the net Laplace pressure gradient in the liquid bulge can be computed as:

$$\frac{dP}{dx} \sim 2\gamma_{LG} sin\theta_{avg} \frac{1}{\delta(x)^2} \alpha$$

where γ_{LG} is the surface tension between liquid and vapour and θ_{avg} is the average contact angle along the length of the bulge.

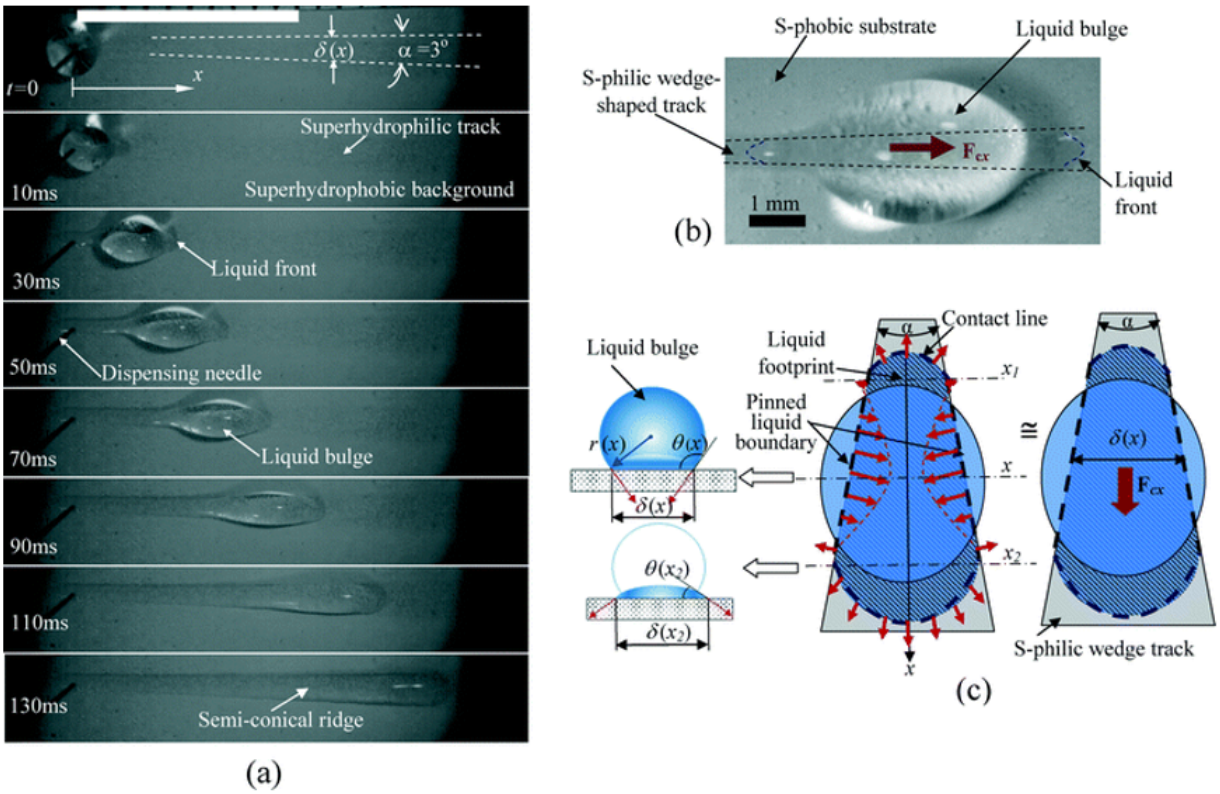

Figure 6: Transport of liquid droplet on wedge shape track: (a) Time-lapsed images (top view) of liquid transport through the wedge-shaped superhydrophilic track on a horizontal Al-substrate. The white bar at the top denotes 10 mm. (b) Morphology of the liquid bulge, approximated as an ellipsoid of finite footprint on the wedge-shaped superhydrophilic track, moving along the track; (c) origin of the driving capillary force on the liquid bulge. (Permission of The Royal Society of Chemistry in Appendix A).

Furthermore, it was noticed that when other droplets are dispensed on a presuffused track (previously wet by the transport of previous droplets), the liquid shape and front behaves as described previously, but they have a velocity higher with respect to the transport of a liquid droplet on a dry track. Moreover, this design is capable of moving the fluid droplet along an inclined plane without any source of power, contributing to the possibility to obtain pumpless 3-D microfluidic systems. A radially outward pattern of divergent tracks was also designed and studied to generate a splitting arrangement, where there is central hydrophilic spot on which is deposited the droplet, and the droplet is uniformly split among the tracks and transported outward.

CHAPTER 2

MATERIALS AND METHODS

2.1 Overview of the Device

In the following section, the general characteristics of the final device are presented and illustrated. The aim of the device is to detect concentrated proteins contained in human body skin oil for a diagnostic purpose on an open-air substrate. Indeed, abnormal increases or decreases in proteins concentration may be a signal of an anomalous health condition that could call for further evaluation. The final device is a few millimeter thick substrate with three main functional regions. Furthermore, each region (outlined below) is characterized by a specific working principle (see Figure 7):

- SAMPLE REGION

  This zone is essentially composed of a "membrane" or a blotting oil sheet (yellow component of Figure 7). Prior to using the device, the user would rub this membrane on their skin, where the membrane absorbs skin oil from the human body. This oil, also known as sebum, is mainly made of proteins and lipids. By depositing a droplet of solvent on the membrane, the solvent can extract the proteins from the membrane and transport them to a “detection zone" for diagnosis.

- TRANSPORT REGION

The design and optimization of this zone are the main focus of the present work. First, the solution of solvent and proteins must be transported from the sample zone to a detection zone. This task is achieved by patterning a specific spatial wettability contrast (wedge-shaped), which allows spontaneous pumpless transport of the fluid (akin to Ghosh et al. [22]). A simple design of wettability patterning is firstly considered: a superhydrophilic wedge shape track confined by a superhydrophobic domain. The capillary force is responsible for the transport of liquid droplets, without requiring an external source of power. The volume of liquid that could be transported on the wettability-confined track is only corresponding to a single a droplet (V $\approx 1\mu$L), but by a cumulative superposition of droplets it is possible to reach a volume up to V ≈ 500 μL.

- DETECTION REGION

  This zone is where the fluid (solution of solvent and proteins) is analyzed. The detection method employed in the present work is the bicinchoninic acid assay, known also as BCA. This biochemical assay technique is commonly employed to quantify the total concentration of proteins in a solution. In the BCA procedure, antigens are immobilized on a solid surface (which has to be functionalized), and all the unbound proteins are removed by washing the substrate several times. The detection is achieved after incubating the BCA reagent with a substrate. The reaction between the BCA reagent and the antigen attached on the surface produces a change in color (from green to purple), which intensity

is subsequently evaluated with a fluorescence microscope. The higher is the intensity of the color, the more pronounced is the concentration of the proteins in the solution.

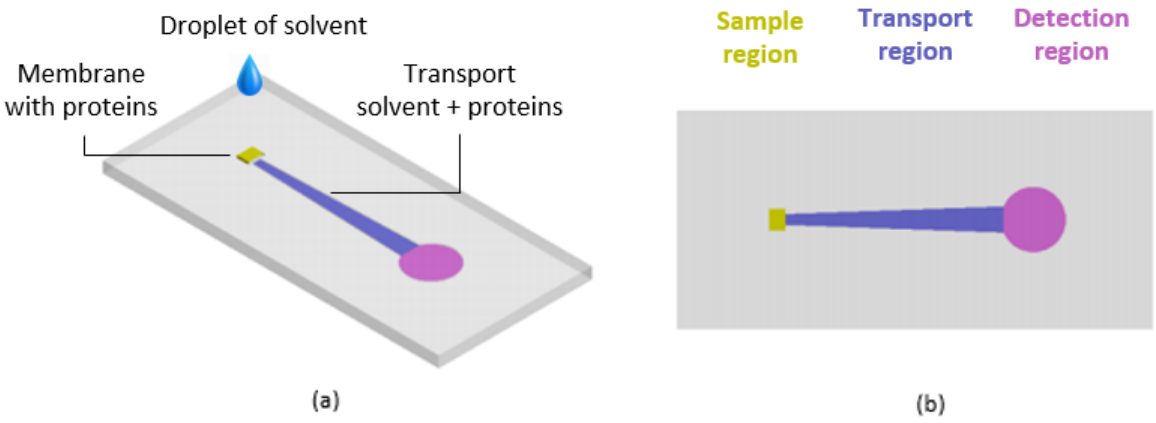

Figure 7: Overview on the final device: (a) isometric view and (b) top view. The yellow region is the sample zone, the blue region the transport zone, and the purple region the detection zone.

Since the focus of this work is on the transport region, which allows the movement of the fluid (solvent and proteins) from the membrane to the detection zone, the sample zone is not considered. In addition, instead of dispensing droplets of solvent that soaks up proteins from the membrane, a solution of solvent and proteins is directly dispensed at the starting edge of the transport track. The solvent used for this purpose is DI water (deionized water), but other solvents may be also employed, such as the Phosphate-buffered saline (PBS). PBS is a water-based salt solution containing mainly sodium chloride and disodium hydrogen phosphate. Moreover, it is a buffer solution commonly used in the biological field because it is able to maintain a constant pH.

2.2 Materials

In the last few decades, the most common materials used in the fabrication of biomedical microfluidic devices were silicon and glass [24]. However, in recent years, polymeric materials have become more popular due to their enhanced mechanical properties and reduced fabrication cost. Substrate material selection depends on the required assay sensitivity and the instrumentation available for signal-detection. The most important properties required for the microfluidic device used in this work is the Ultraviolet (UV) light and the visible light transparency. These properties are crucial to quantify the fluorescence under an inverted fluorescence microscope with diascopic (transmitted) illumination. Indeed, the detection of the proteins contained in the fluid is accomplished by means of the BCA procedure, whose last step is the color change production and detection by means of a inverted fluorescence microscope. In this type of mi-

croscope, the illumination source is located above the sample and the direction of the light rays is controlled by a group of mirrors. The transparency of the substrate is required to allow the light to pass through the substrate, ultimately reaching the lens located below the sample.

Hence, the materials selected for the substrate are polycarbonate and glass. Besides being transparent, these materials are commonly used in the biomedical industry to produce Lab-on-chip and Point-of-care devices. It is necessary to underline that, at the beginning of this work, the attention was focus on two materials instead of one, in order to have two different possibilities to perform the functionalization.

2.3 Detection of Proteins

As mentioned previously, during the device prototyping step, the BCA Protein Assay is performed. This is a detergent formulation based on bicinchoninic acid (BCA) for the quantification of total antigens by means of a calorimetric detection protein. First, antigens (bovine serum albumin (BSA) was used in this work) are attached to a functionalized substrate (functionalization is needed for immobilization). BCA is then added and incubated. If any antigens (BSA) were successfully immobilized on the substrate, a color change is produced (from green to purple) and the intensity of the color is proportional to the total amount of antigens adsorbed by the functionalized substrate. The protein concentration is determined by taking into account a standard curve as well. In the BCA assay, it is not possible to capture a specific protein, but instead, all antigens are detected. Therefore, this technique cannot harness specificity of protein detection

and thus is merely used as a proof of concept: the BCA method will work as well as other immunoassay techniques on a surface which has been correctly functionliazed, i.e. made bioactive. It is important to note that the BSA protein was chosen is this work as model for all proteins that are typically found in skin oil. The final solution used to simulate the skin oil is composed by 1% BSA, added to a pre-mixed solution of 4 mg/mL 1-ethyl-3-[3-dimethylaminopropyl]carbodiimide hydrochloride (EDC) and N-hydroxysulfosuccinimide (SNHS) in a concentration of 11 mg/ml [25].

The BCA procedure follows these steps:

- Incubation of the solution (solvent and proteins) for 1 hour at 37 °C.
- The substrate is washed with DI water and dried with nitrogen 5 times, in order to remove all the unbounded antigens.
- The working reagent is prepared by mixing 50 parts of BCA reagent A with 1 part of BCA reagent B (50:1, Reagent A,B). The color of the solution is green at this point.
- The BCA reagent obtained in the above step is deposited on the functionalized substrate and incubated for 30 min at 37 °C. A color change is produced (green to purple) if BSA proteins are present on the substrate. Otherwise, if no proteins are detected the color remains green. The intensity of the color is proportional to the concentration of the antigens in the solution.

2.4 Substrate Functionalization

Surface functionalization is an efficient method used to manipulate the surface properties of a substrate to obtain a specific objective, such as an effective bioresponse, and the study of substrates functionalization gained a lot of interest in the past few decades especially in the biomedical field. This is due to the importance of functionalization procedures to make biocompatible materials. In the present work, the attention focuses on a surface functionalization procedure that allows the interaction between proteins and the surface. The mechanisms of protein-surface interaction are not fully understood, nevertheless it is worth to mention some chemical characteristics of both proteins and surfaces that can affect this phenomenon [26]:

- Stability, size, concentration of proteins and protein-protein interactions;
- Free energy of the surface substrate (hydrophobic/hydrophilic properties and polarity);
- Surface charge (related electrostatic interactions);
- Chemical nature of surface functional groups;
- Biological surrounding (pH, temperature, *etc.*).

There are different surface functionalization strategies that can be used on various solid substrates, including glass, polymeric and metallic materials. The functionalization methods used for glass and polycarbonate have been proven to be both effective and easy to impliment. In the following sections, the two functionalization procedures are described.

2.4.1 Glass Functionalization

The glass is functionalized with an aminosilane treatment (APTES) in order to make possible the proteins adsorption by the surface. The protocol is mainly divided in two parts [27]:

- Reagent preparation and glass cleaning

  A pre-cleaned glass microscope slide (dimensions 25x75x1 mm; Thermoscientific clipped corner plain) is placed in an oxygen plasma machine for 5 min at 50% of the power. A solution of 2% reconstituted APTES is prepared, by adding 50μL of APTES in 2.45 mL of ethanol in a conical tube.

- APTES functionalization

  Pipette 2.30 mL of APTES solution onto the surface for the glass microscope slide in order to create a thin liquid film. The surface is covered with a plate to prevent the evaporation of the solution, and it is placed on a platform shaker for 50 minutes at room temperature to create a homogeneous and smooth APTES layer. The glass slide is then rinsed three times with 2.30 mL of pure ethanol, by pipetting at a 70° angle. The sample is dried with nitrogen gas and placed in an oven at 90° C for 1 hr.

2.4.2 Polycarbonate Functionalization

Similar to glass functionalization, the polycarbonate is also functionalized with an aminosilane treatment (APTES), but the procedure is slightly different [25]:

- A clear impact-resistant polycarbonate sheets with a thickness of 1/16" is cut in smaller pieces of dimensions 25x75x1 mm.

- Each plate is immersed in glassware (8 cm diameter) with 50 mL of pure ethanol at 37° C for 5 min, followed by 5 washings with DI water.
- Each plate is then placed in glassware with 50 mL of potassium hydroxide (KOH) solution (1.0% w/v in DI water) for 10 min at 37° C and then washed 5 times with DI water.
- The KOH-treated substrate is then treated with O_2-plasma for 3 minutes .
- The substrate is then functionalized with amino groups by incubating it in 50 mL solution of APTES (2 % v/v in DI water) at 80° C for 40 min. Subsequently, the sample is placed in a desiccator for 1 hr 40 min in order to achieve maximum surface silanization. The amine-functionalized substrate is washed 5 times with DI water in order to remove all the excess unbound APTES from the surface.

In order to test the effectiveness of the functionalization procedure, protein detection is performed with the BCA method mentioned above (as shown in Figure 8). If the substrate is correctly functionalized, the reagent turns purple after BCA deposition onto amine-functionalized substrates. On other hand, if the substrate is not functionalized, no proteins are present after washing, and the reagent remains green.

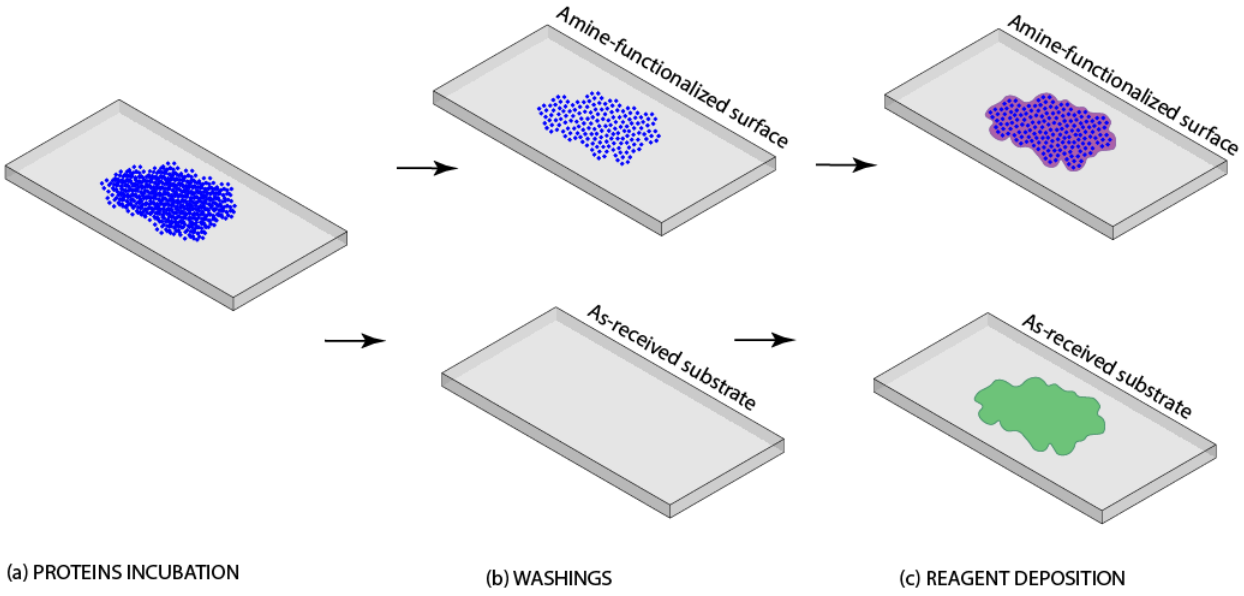

Figure 8: Protein immobilization procedure: (a) proteins solution incubated for 1 hour at 37 °C, (b) the substrate is washed 5 times and if the surface is properly functionalized, the proteins are immobilized. Otherwise they are washed away. (c) The reagent is deposited on the substrate and changes color from green to purple if proteins are present on the substrate.

CHAPTER 3

DESIGN OF THE TRANSPORT REGION

3.1 Wettability Characterization of the Transport Region

Before the study of using wettability patterning for pumpless transport of a fluid, it is necessary to analyze the properties of the surface of the silane-functionalized substrate. In particular, attention is focused on the wetting regimes of the silane-functionalized glass and polycarbonate surfaces.

The wettability (*i.e.* contact angle (CA)) of glass and polycarbonate surfaces are both altered through silane treatment. The pre-cleaned glass microscope slide has a contact angle of approximately 0 °, however, this contact angle is very sensitive to the contamination. For example, the contact angle of an "as-received" glass slide usually ranges between 8 °and 18 °due to grease and/or dust present on the surface. After the silane-functionalization procedure, the contact angle of the glass becomes approximately $78^\circ \pm 2.8^\circ$ (compared to 0 °for pre-cleaned glass). This value is computed by taking into account 6 different silane-functionalized glass substrates, for each of which the contact angle is calculated by considering 5 locations and computing the average and standard deviation. Since, the contact angle of a water droplet on a pre-cleaned glass substrate is not defined, Figure 9 represents only the static CA of a droplet on the silane-functionalized glass.

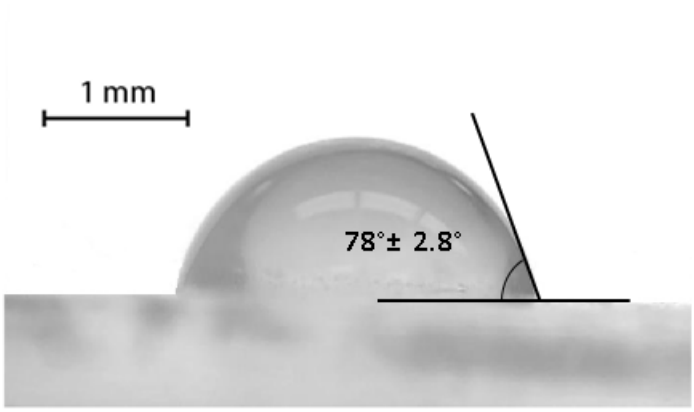

Figure 9: Static contact angle for a water droplet on a silane-functionalized glass substrate.

As for the polycarbonate susbtrates, before silane-functionalization, the contact angle is $83.8^\circ \pm 1.3^\circ$. This value is obtained by computing the average of contact angles of five locations on the same polycarbonate substrate and by calculating the average and standard deviation. After the silane-functionalization procedure, the contact angle becomes $65^\circ \pm 2.6^\circ$. This value is computed by taking into account 6 different silane-functionalized polycarbonate substrates, where the contact angle is determined by the average of 5 values and computing the standard deviation. The main difference in CA of the as-received and silane-functionalized polycarbonate is illustrated in Figure 10.

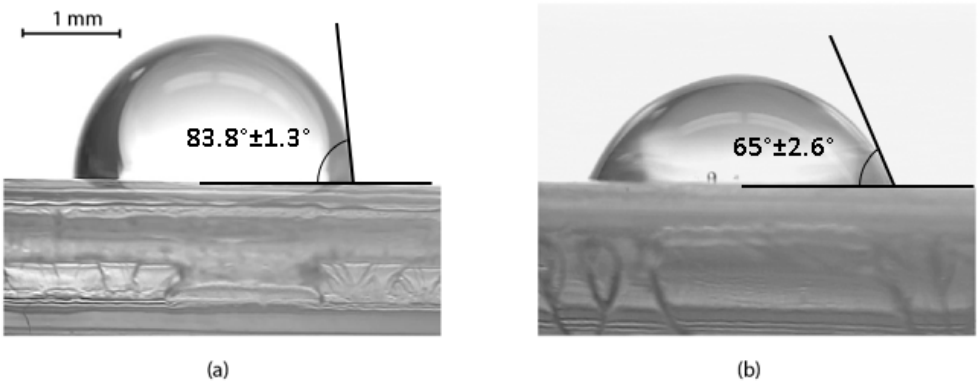

Figure 10: Static contact angle for a water droplet placed on (a) as-received polycarbonate substrate and (b) amine-functionalized polycarbonate substrate.

The results of both the analysis demonstrate how the contact angle of the amine-functionalized polycarbonate tends to be smaller (*i.e.* more hydrophilic) with respect to that of the amine-functionalized glass. Once the wettabiliy of the substrates used in this work was fully understood, wettability patterning could be carried out on the substrates. In this recent years, different approaches have been proposed to impart a wettability gradient on surfaces to control droplet motion on substrates [28]. Xing et al. [29] introduced the concept of the spontaneous transport of a liquid on a wettability patterned substrate: superhydrophilic track on superhydrophobic domain. In this case, the driving force is provided by Laplace pressure. This concept

is utilized for the design of the transport region in our work.

Instead of differentiating between a transport and a detection zone, the two regions are combined into a single one: the transport is performed on the detection zone (amine-functionalized for protein immobilization). Hence, a superhydrophilic track (typically used for the fluid transport on wettability-patterned substrates) is substituted with a amine-functionalized track. In both the cases of glass and polycarbonate, the silane-functionalized track results to be hydrophilic (CA < 90 °). Thus, instead of having a high-contrast, wettability-patterned substrate, the substrate used in this work is composed of a hydrophilic, silane-functionalized track on a superhydrophobic background.

3.2 Device Fabrication and Wettability Patterning Procedure

Wettability patterning via a coating method is generally substrate independent (metals, polymer or paper). In the present work, the same coating procedure is used for both substrates: glass and polycarbonate. In order to obtain a non-wettable domain on the substrates, the following procedure is employed [30]. A dispersion containing TiO_2 nanoparticles, perfluoroalkylmethacrylate copolymer (PMC) (Capstone ST-100, 20 wt. % in water; DuPont®), ethanol, and acid acetic is prepared and the solution is sprayed-deposited onto the surface of the substrate. In particular, for a typical batch, 0.5 g of titanium dioxide anatase TiO_2 nanoparticles ($\leq$ 25nm, Sigma-Aldrich) is dispensed in 6 gr of ethanol (Decan Labs) and 0.625 g of Acid Acetic. Once these components are added, the dispersion created is hand shaken at room temperature and

probe-sonicated with an energy supplied equal to 1000 J (13 mm probe diameter, 750 W, 40% amplitude, Sonics Materials Inc., Model VCX-750). After sonication, 0.625 g of hydrophobic PMC is immediately added to the mixture. The above solution is shaken mechanically in order to obtain a stable dispersion. Subsequently, it is left stabilize for approximately 24 hours. After stabilizing, the solution is sprayed onto the substrate using an siphon feed airbrush (o.73mm spray nozzle diameter, 275 kPa air pressure, VL-Set, Paashe) from a distance of 30 cm in order to obtain an uniform coating. After this procedure, the final coating is superhydrophobic ($\theta_{water} \sim 160^{\circ} \pm 2^{\circ}$) because of the combination of the hydrophobic PMC (a very thin film which has a contact angle $\theta_{water} \sim 117^{\circ}$) and the TiO_2 that increases the roughness. The concentration of TiO_2 and PMC are determined in order to obtain the optimal mass fraction of 0.8. The mass fraction is calculated as:

$$\phi = \frac{m_F}{m_F + m_P}$$

where m_F is the mass of the filler (TiO_2), and m_p the mass of the polymer (PMC) on a dry basis.

Since we need to maintain an unaltered amine-functionalized hydrophilic track, before spraying the dispersion, it is necessary to cover the region of interest. In order to achieve this task, a wedge-shaped masked is cut from blue painters tape and is attached on the substrate as represented in Figure 11.

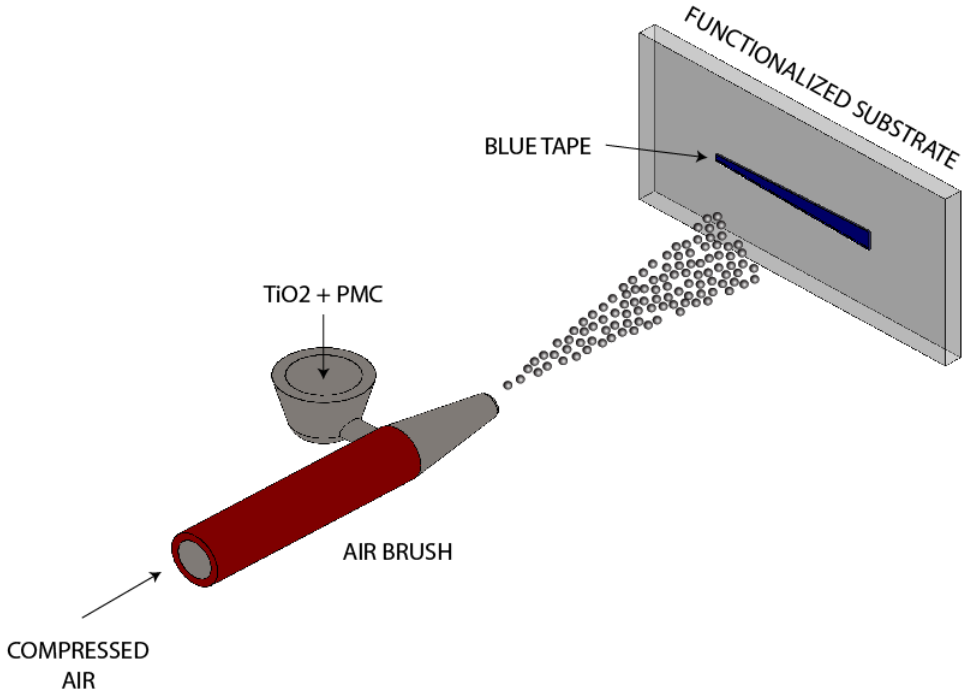

Figure 11: Salient steps of the surface coating: Spray of TiO_2-PMC suspension on the amine-functionalized substrate to form the superhydrophobic background. A wedge-shaped mask (made from blue painters tape) is positioned on the substrate to cover and protect the amine-functionalized region.

After the coating procedure, the tape is removed from the substrate. The final configuration of the design is the wedge-shaped amine-functionalized track (hydrophilic) on a superhydrophobic domain (Figure 12).

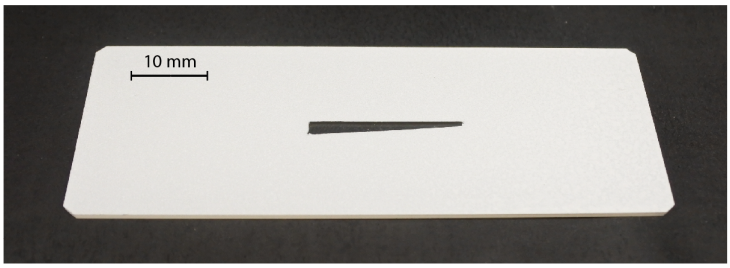

Figure 12: Wedge-shaped amine-functionalized track on a TiO_2:PMC superhydrophobic background.

3.3 Limitation of a Single Wedge Track

The transport on this wettability pattern is analyzed in both the cases of amine-functionalized polycarbonate and glass tracks (Figure 13). The results are compared with the ones obtained in the case of supehydrophilic tracks. The tracks on the various substrates feature the same geometry, where the wedge angle is chosen $\alpha = 3°$. The narrowest edge where the droplets begin to be transported has dimension 500 μm, while the length of the track is 2 cm.

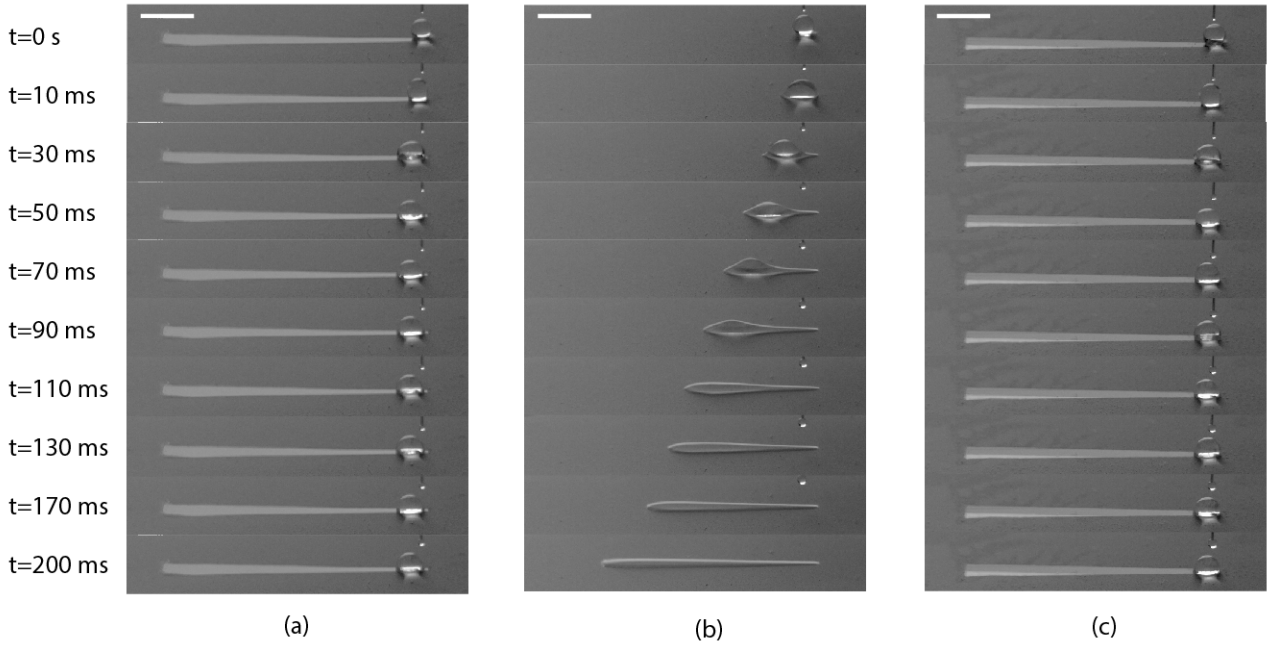

Figure 13: Time-lapsed images of liquid (BSA+DIW) transport through a (a) wedge shape amine-functionalized polycarbonate track, (b) wedge shape superhydrophilic track, and (c) wedge shape amine-functionalized glass track. The white bar at the top denotes 5 mm.

The above figures show the behavior of the droplets when it is deposited on the narrowest edge of the tracks. As can be seen from Figure 13, liquid transport along the amine-functionalized polycarbonate and glass tracks is not possible, although it is possible for the case of the superhydrophilic track. This behavior is due to the fact that there is not enough wetta-

bility contrast between the track and the surrounding region. Due to this transport limitation on the single amine/functionalized track other design alternatives we explored.

3.4 Introduction of Different Designs

The main outcome of the previous section is the inability to transport fluid on the amine-functionalized glass or polycarbonate wedge-shaped tracks. Therefore, alternative track designs are evaluated to overcome this limitation. The analysis is carried out only for the case of amine-functionalized polycarbonate, because of its lower contact angle compared to that one characteristic of the amine-functionalized glass ($65^\circ \pm 2.6^\circ$ instead of $78^\circ \pm 2.8^\circ$). This allows for higher wettability contrast between the silane-functionalized region and the superhydrophobic background. Three different designs are introduced:

- DESIGN 1: Wedge-shaped superhydrophilic track with a circular amine-functionalized reservoir at the end, all laid in a superhydrophobic background.
- DESIGN 2: Wedge-shaped superhydrophilic track in a superhydrophobic domain. The amine-functionalized is laid directly on the transport track, as a sort of island.
- DESIGN 3: Amine-functionalized axial track is located between two symmetric superhydrophilic tracks, all laid on a superhydrophobic background.

In the proposed solutions the detection zone is separated from the transport region, with the intention on fulfilling the geometrical constraints imposed by the problem. The size detection zone has to be larger than at least 10 mm^2, and this constraint is imposed by the fluorescence

microscope detection capability. Different designs are illustrated in the following section and a new design parameter is introduced to select the optimal configuration that allows both liquid transport and detection. Figure 14 shows the first proposed design (Design 1), which is mainly characterized by the following features:

- Transport Region: wedge-shaped superhydrophilic track on the superhydrophic domain. The fluid (solvent+proteins) spreads in the transverse direction constricted by the wedge boundary.
- Detection Region: circular reservoir with a characteristic diameter 3.5 mm positioned at the end of the track. The fluid reaches the widest edge of the track and then it spreads in the reservoir.

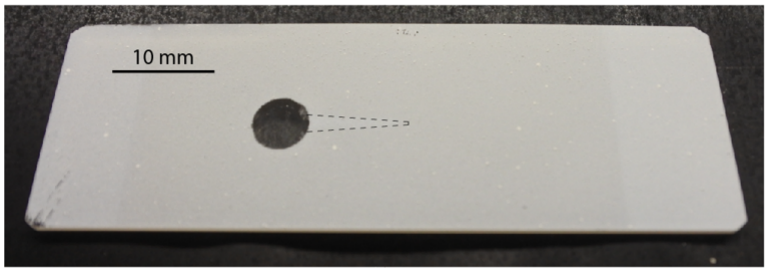

Figure 14: Superhydrophilic wedge-shape track (marked by dashed line) on a superhydrophobic domain (white region) with a circular amine-functionalized reservoir placed at the end.

The substrate shown in Figure 14 is made using the following procedure, which is also shown schematically in Figure 15:

- A circular piece of tape is positioned on a amine-functionalized polycarbonate substrate to cover and avoid altering the reservoir. The dimension of the tape correspond to the reservoir dimensions.
- Spray-coating of the TiO_2 :PMC dispersion onto the masked substrate, as described in the previous section. After spraying, a composite is formed on the substrate that makes it intrinsically superhydrophobic.
- The tape is removed so that a silane-functionalized, circular reservoir is revealed. The superhydrophilic track is directly formed on the superhydrophobic surface by taking advantage of the photocatalytic nature of Anatase TiO_2 under UV exposure. Thus, the coated substrate is exposed to UV radiation ($Dymax^{TM}$ 5000 EC, 390 nm UV wavelenght, 400 W UV lamp) for 30 minutes using a polyethylene teraphthalate (PET) photomask printed with black negative patterns using a common laserjet printer. The UV light can pass through the transparent region of the photomask (unprinted), promoting a photocatalic conversion of the UV-exposed regions and rendering them superhydrophilic, while the properties of the unexposed region are conserved (remain superhydrophobic).

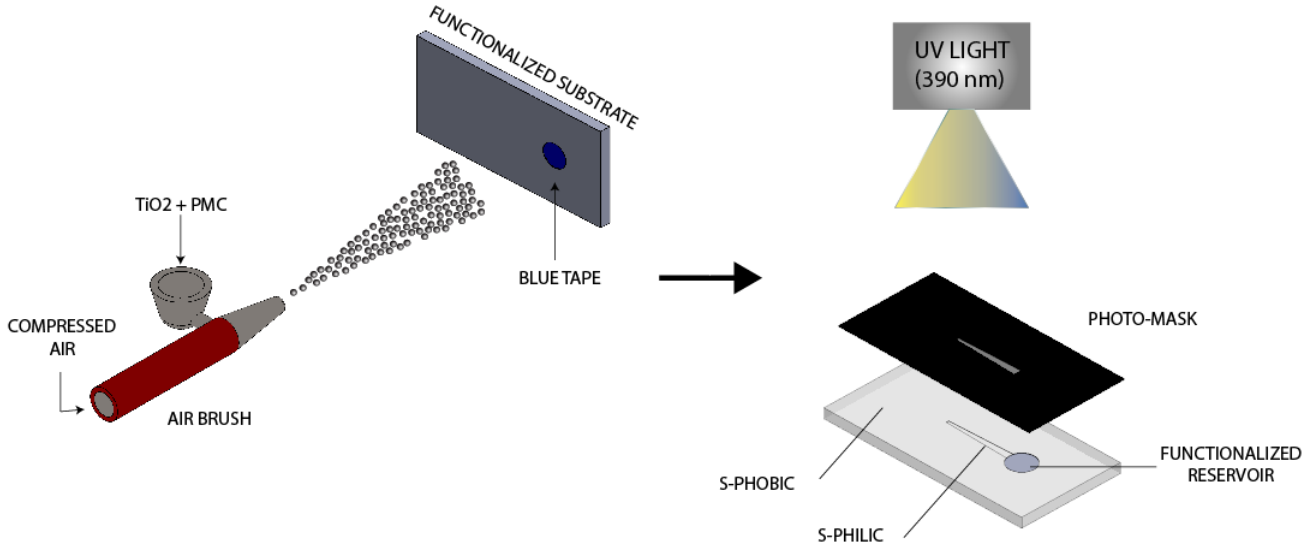

Figure 15: Spray coating of the TiO_2-PMC dispersion onto the silane-functionalized substrate to make the surface superhydrophobic. A circular piece of tape is positioned onto the substrate to mask a circular-shaped region during the spray process. Subsequently, UV treatment of the superhydrophobic surface through a photo-mask (top) to create the superhydrophilic track (bottom). The exposed region turns to be superhydrophilic after 30 minutes of exposure to UV light, while the unexposed domain remains unchanged.

The liquid transport on this type of tracks is analyzed in Figure 16. The liquid spreads along the transverse direction if the wedge-shaped track, constricted by the wedge boundary, and its front propagates until reaching the end of the superhydrophilic track (*i.e.* the boundary between the track and the reservoir). By dispensing several droplets the propagating front remains approximately at the same position while the height of the bulge increases. The liquid is not transported into the reservoir (detection zone) until enough liquid is dispensed (greater than 39.9 μL or 3 droplets) This behavior is due to the high wettability contrast between the track (superhydrophilic) and the amine-functionalized reservoir (hydrophilic: CA $\sim$ 65 °for polycarbonate). In this case the transport results to be discontinuous between the track and the reservoir. The liquid rests at the end of the track and it spreads in the detection region only when the Laplace pressure difference is high enough to overcome the contrast in wettability between the track and the reservoir.

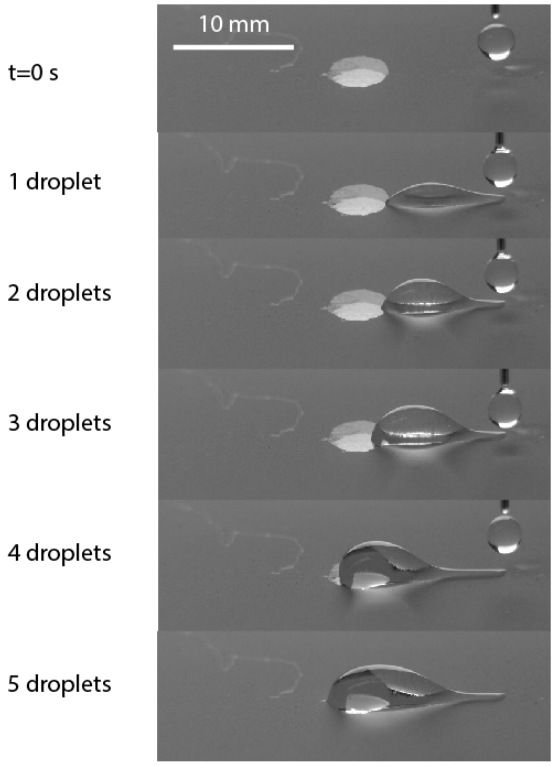

Figure 16: Time-lapsed images of droplets dispension and liquid transport through the wedge-shaped superhydrophilic track with the amine-functionalized reservoir placed at the end.

After having observed this behavior, other design ideas were proposed (Design 2). The second design alternative features the amine-functionalized reservoir directly on the transport track, as a sort of transparent, hydrophilic island laid on the superhydrophilic region (Figure 17).

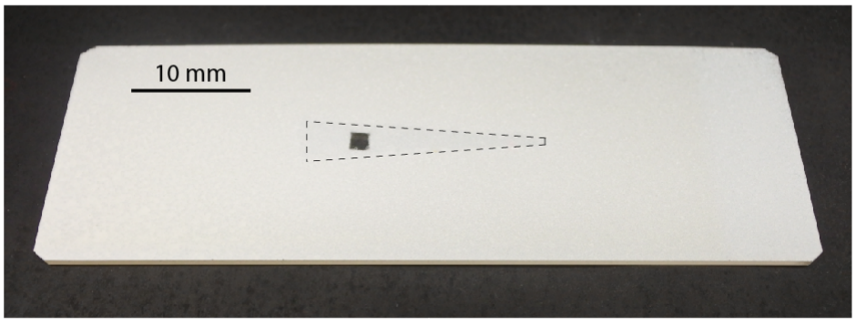

Figure 17: The amine-functionalized island laid on the superhydrophilic wedge-shape track (surrounded by dashed line) on a superhydrophobic domain (white region).

The shape of the reservoir is a 9 mm^2 square, whose dimension is dictated again by the fluorescence microscope imaging constraint. In order to obtain this configuration, a similar procedure to the one explained in the previous design, was used. Thus, a square piece of tape is attached on the silane-functionalized substrate, the spray coating of the TiO_2-PMC dispersion is performed, and the tape is removed. Then, the substrate is exposed to UV radiation by using a different photomask. The main difference here is represented by the photomask employed, where a black region, correspondng to the reservoir position, is printed where the respective transparent region is. In this way, the amine-functionalized zone is not exposed under the UV light.

The transport behavior of this design is very similar to the first design. Indeed, the liquid spreads along the transverse direction of the superhydrophilic track, constricted by the wedge

boundary. The front of the liquid propagates until reaching the first edge of the transparent island (detection zone), where it stops at the boundary between the superhydrophilic region and the amine-functionalized region. While dispensing several droplets, the front remains approximately at the same position while the height of the bulge increases. When the Laplace pressure gradient is high enough to overcome the contrast in the wettability between the track (superhydrophilic) and the amine-functionalized reservoir (hydrophilic: CA $\sim$ 65 °for polycarbonate), the liquid spreads into the silane-functionalized region and propagates to the end of the track. These events can be seen in Figure 20.

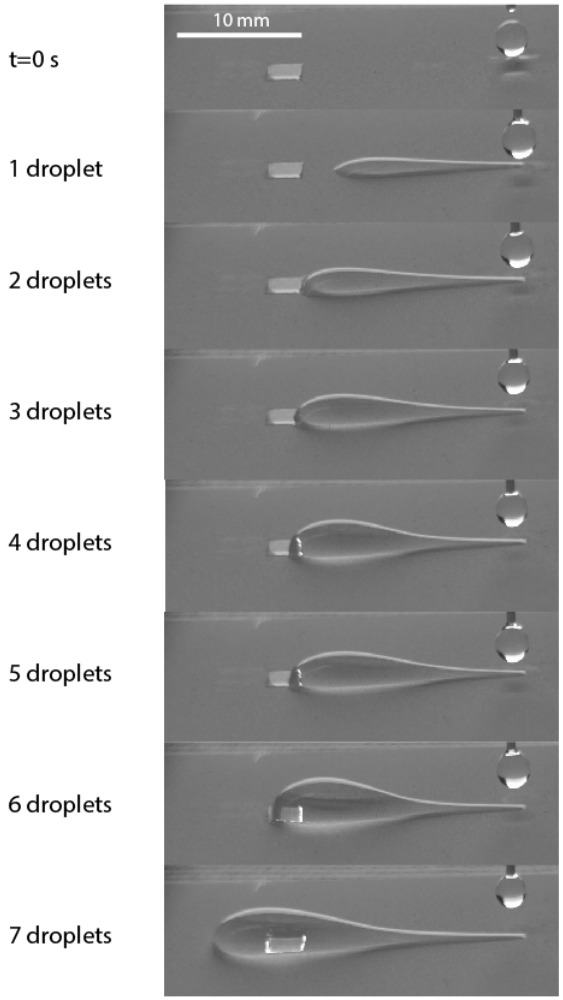

Figure 18: Timestamps capturing the dispensing and transport of the liquid (water) through the wedge-shaped, superhydrophilic track with a silane-functionalized island laid on it.

Due to the fact that liquid transport into the detection zone of designs 1 and 2, the last design proposed (design 3) is a patterned surface containing 3 wedge-shaped adjacent tracks with the same divergence angle and the same starting vertex (see Figure 19). The two external tracks are superhydrophilic, while the internal track is amine-functionalized (CA $\sim 65°$). In the subsequent sections, the internal track is referred to as axial track.

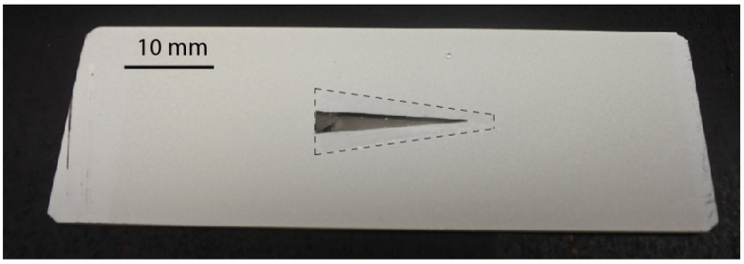

Figure 19: Triangular amine-functionalized transport reservoir placed between two superhydrophilic tracks.

The procedure to obtain this design is very similar to that described for the two previous designs and is shown schematically in Figure 20.

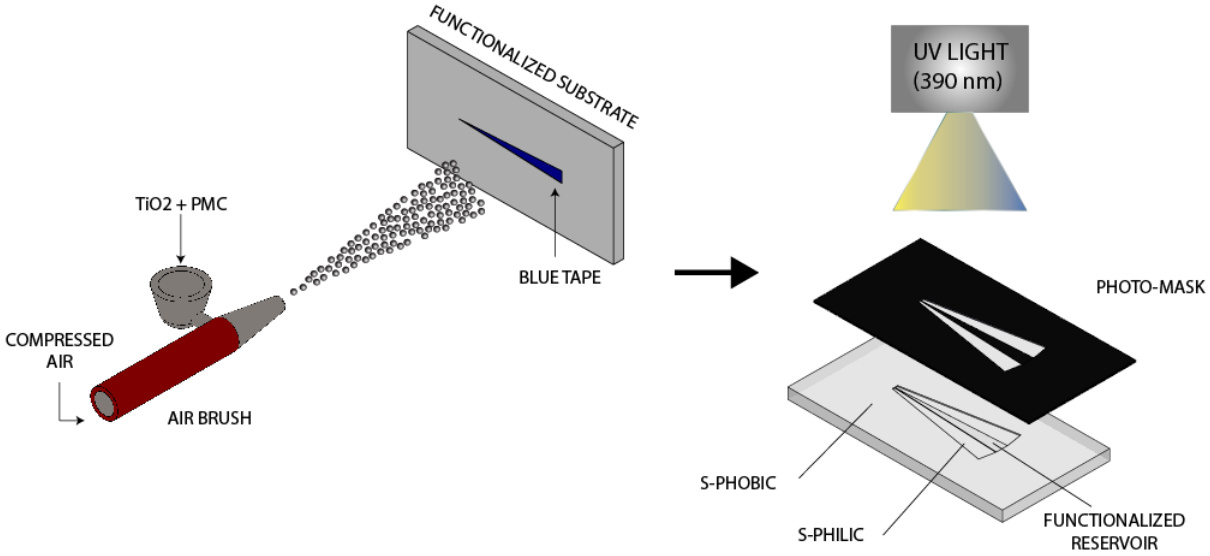

Figure 20: Spray coating of TiO_2-PMC dispersion on the amine-functionalized substrate to form the superhydrophobic surface. A wedge-shaped piece of tape is placed on the substrate to cover the amine-functionalized region prior to spraying. Subsequently, UV treatment of the superhydrophobic surface with a photo-mask placed on the top of the substrate. The transparent region of the mask allows the formation of the superhydrophilic tracks.

The transport for this design is shown in Figure 21. When one droplet is dispensed at the vertex, it moves along the tracks due to the unbalanced force (Laplace pressure gradient). Thus,

the liquid spreads and stops in the position at which the equilibrium of forces is reached. This final position can vary according to both the wedge angles of the superhydrophilic tracks and the axial track.

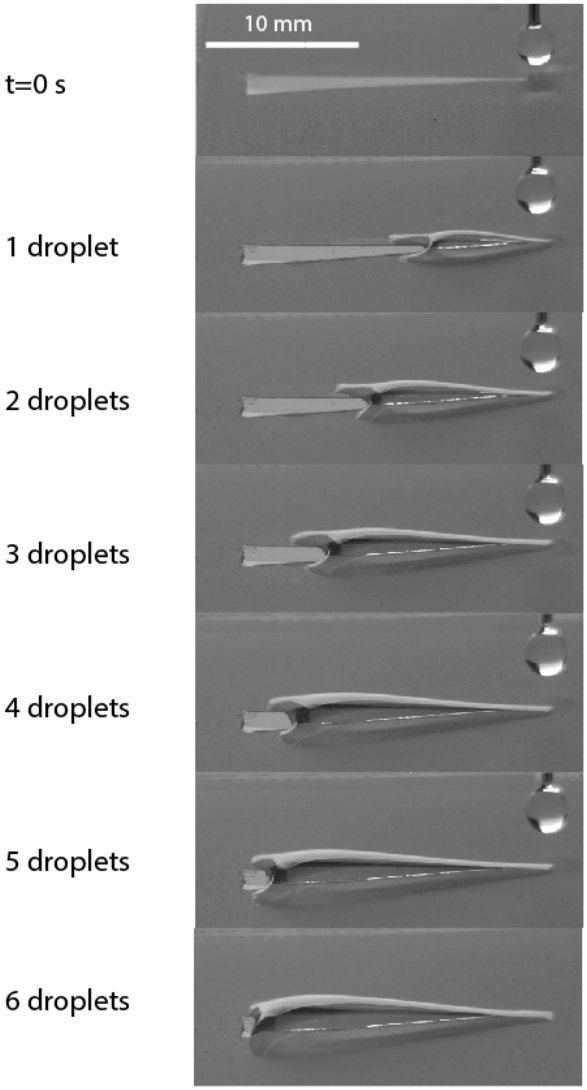

Figure 21: Timestamps showing the liquid transport through the 2 wedge-shaped superhydrophilic tracks sandwiching an amine-functionalized reservoir in the middle.

In order to evaluate the optimal design, a new parameter (or optimization factor) is introduced that takes into account the volume of liquid dispensed and the detection area. This optimization factor is defined as:

$$r = \frac{V}{A_d} \quad [mm]$$

where V is the dispensed volume and A_d is the surface area of the silane-functionalized track. The extension of the detection area and the number of water droplets dispensed are known for all three designs. In each case, the liquid is dispensed by using a dispensing needle (internal and external diameters respectevily 0.41 mm and 0.72 mm). The total volume can be determined by multiplying the volume of one single droplet times the number of droplets dispensed. The volume of one droplet is determined by weighing n droplets, dividing by the density (ρ = 997 kg/m^3), and dividing the obtained result by n. Once the volume is known, it is possible to calculate the droplet equivalent diameter d_{eq}, defined as the diameter of a sphere having the same volume of the droplet. The volume of a single droplet dispensed by the dispensing needle is V = 13.33 μl, and corresponding to d_{eq} = 2.94 mm. At this point, d_{eq} must be compared to the capillarity length, indicated as k^{-1}. The value of k^{-1} defines the threshold beyond which gravity becomes important: if $d_{eq} < k^{-1}$ the effect of gravity can be neglected [1]. This value is computed by equating the hydrostatic pressure $\rho g k^{-1}$ of a liquid with density ρ at a depth k^{-1} submitted to the gravity g=9.8 $\frac{m}{s^2}$ and the Laplace pressure defined as $\frac{\gamma}{k^{-1}}$. Thus, the capillary length is defined as:

$$k^{-1} = \sqrt{\frac{\gamma}{\rho g}}$$

Generally, the capillary length is of the order of few millimeters. To increase the value of k^{-1} of a liquid, it is necessary to work in micro-gravity environment or to replace air with a liquid having a density similar to that of the original liquid. In the case of water $k^{-1} \approx 2.7$ mm. In the case of the dispensing needle used in this work, the diameter of the droplet is higher that the capillary length, and thus gravity can't be neglected. The effect of gravity can be limited by placing the needle as close to the narrowest edge of track as possible, but avoiding that the droplet touches the track before its detachment from the tip of the needle. In Table I, the values of r are presented for all the proposed designs. For low r, the smaller amount of liquid is needed to be dispensed in order to cover a unit surface area of the reservoir. Given the necessity of minimizing the amount of liquid to be dispensed (due to solution cost and availability), and thus the solution containing the antibodies, r must be as low as possible.

TABLE I: OPTIMIZATION FACTOR r

Design	A_d **[**mm^2**]**	**n**	**V [**μ**L]**	r $[mm]$
First design	9.62	5	66.5	6.91
Second design	9	7	93.1	10.34
Third design	21	6	79.8	3.8

As seen in Table I, A_d is the surface area of the detection zone, n the number of droplets, and V the volume dispensed. It is possible to note that the lower r value is obtained by employing the solution with the triangular reservoir placed between the two superhydrophilic tracks. Therefore, this is the design which was selected.

CHAPTER 4

RESULTS AND DISCUSSION

4.1 Protein Detection on the Axial, Amine-Functionalized Track

Once the design for the transport region was optimized (design 3, see previous section), a protein detection study was performed on the axial, amine-functionalized track (BCA method is used to detect the BSA proteins). To begin, a solution of EDC 4 mg/mL and (N-hydroxysulfosuccinimide) SNHS 11 mg/ml is incubated for 15 min at 37 °C. Afterward, 1% BSA is added to the pre-mixed EDC+SNHS solution. Then, one droplet of this solution is deposited at the narrowest edge of the axial track and it is transported via a Laplace pressure gradient along the length of the track. When the net force acting on the droplet vanishes, the front of the liquid stops at a certain axial position (x) that corresponds approximately to $\frac{5}{12}$ of the total length (20 mm). The distance covered by the liquid depends mainly on the diverging angles of both the axial track and the superhydrophilic tracks on either side of the track, and one droplet isn't enough for the liquid to reach the end of the design. Hence, more droplets of liquid have to be dispensed in order to cover the entirety of the detection area of the amine-functionalized track. When the first droplet reaches the maximum axial distance, a second droplet of the same size is dispensed, and so on until the liquid covers the entire detection region. The total amount of droplets needed to obtain the entire coverage of the amine-functionalized track is 6, which corresponds to a total volume of liquid $V_{tot} \approx 79.8$ μl. The transport happens as shown in Figure 21, and after the

transport events, the substrate is incubated at 37° C for 1 hour. Then the substrate is washed and dried five times with DI water to remove any residual unbound proteins. Finally, the BCA procedure is performed by dispensing BCA reagent onto the diverging track and the color of the reagent changes from green to purple, indicating the presence of proteins attached on the amine-functionalized region.

If the same procedure is performed on as-received polycarbonate (*i.e.* not silane-functionalized), the BCA solution would not change color, indicating that no proteins remain attached to the axial track after washing. On the other hand, the experimental results tend to be different. Indeed, in both the cases (amine-functionalized and as received substrate) the reagent exhibits the same purple color as illustrated in Figure 22. However, we must consider that the BCA reagent is being transported via superhydrophilic tracks composed of anatase titanium dioxide. It is known that this form of TiO_2 is photocatalytic when exposed under the ultaviolet light. Recently, the photo-functionalization of TiO_2 has been studied and acquired a great importance in the biological field due its chemical alterations. Interestingly, the photochemical reaction of the anatase TiO_2 does not only make the transport tracks superhydrophilic, but it also increases the bioactivity of the tracks in terms of proteins adsorption capability or cellular attachment [31],[32],[33],[34]. In order to verify this, a simple experiment was performed, where the detection procedure is directly performed on a single superhydrophilic wedge-shaped track. Here, the track (bioactive due to TiO_2) is able to absorb proteins, and thus after the BCA deposition, the

reagent changes color from green to purple (see Figure in Appendix B).

The color change in the substrate shown in Figure 22-b, where the axial track is not amine-functionalized, is thus justified by the changing in the bioactivity of the TiO_2. Even though proteins are present on the superhydrophilic tracks, they cannot be detected under the transmitted fluorescence microscope because those regions are not transparent (due to the TiO_2 coating). Therefore, the transparent amine-functionalized region is needed for the detection task (Figure 22-a). Moreover, since the protein concentration is an intensive property (it does not depend on the size of the system), it can be determined by looking only at the amine-functionalized region regardless of the fact that proteins are also present on the superhydrophilic tracks. Hence, this configuration (design 3) is selected as final design for the present device.

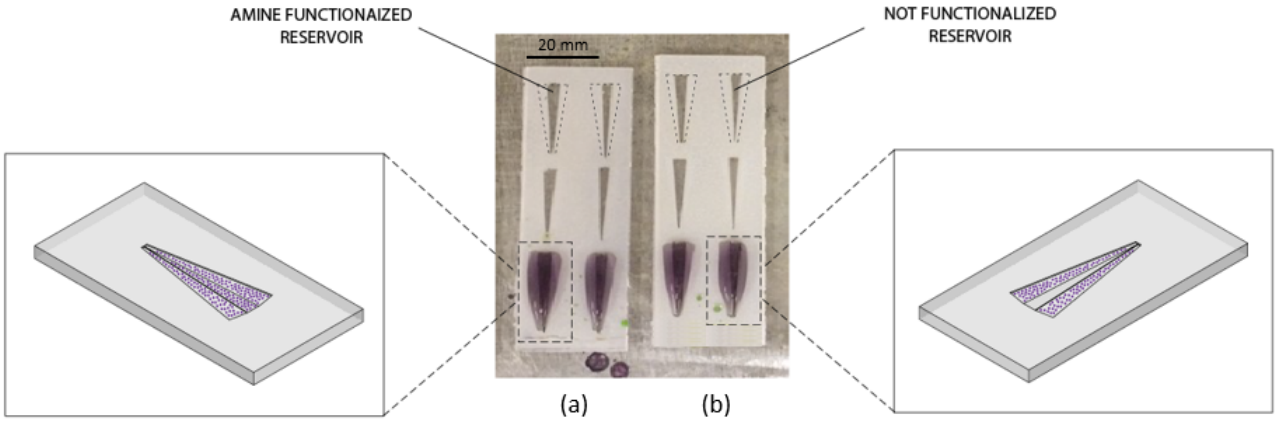

Figure 22: Proteins are present on (a) the silane-functionalized axial and superhydrophilic tracks and (b) only on the superhydrophilic tracks. The insets of (a) and (b) show the expected binding sites for the proteins.

4.2 Design Optimization

The objective of this section is to choose the best parameters for the selected design in order to have optimal liquid transport. Once the droplet is dispensed at the narrowest edge of the track, it spreads in the lenghtwise direction. Due to the presence of the amine-functionalized track (hydrophilic) between the superhydrophilic tracks, the liquid is not able to move completely to the end of the track. Figure 23-b represents the liquid bulge after dispensing three droplets

($V_{tot} \approx 39.9\ \mu$L). It is important to note that the propagation front (shown at x mm in Figure 23-b) assumes the characteristic shape of a parabola with the concavity facing the end of the track. This shape is consequence of the fact that the liquid spreads completely in the superhydrophilic tracks while it tends to "stick" on the amine-functionalized region (due to being hydrophilic). It is as if the fluid on the superhydrophilic tracks drags the liquid over the hydrophilic track (similar to pulling a rain cover over a tent).

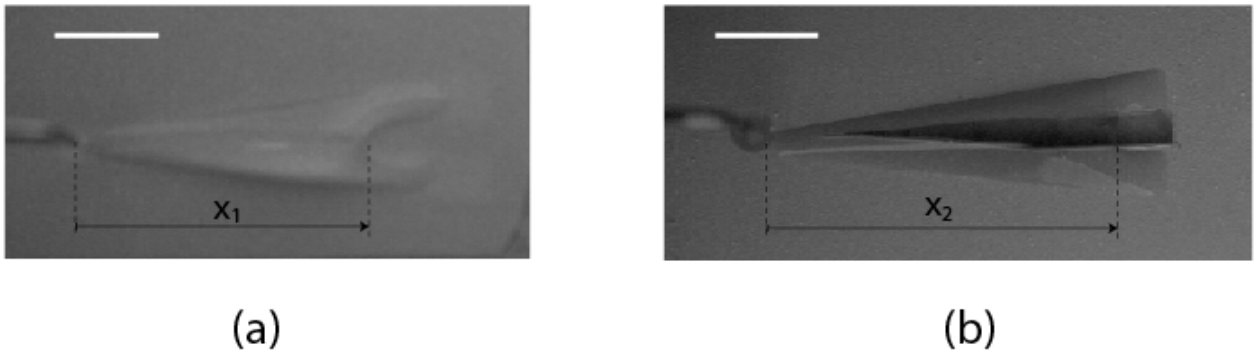

Figure 23: Characteristic shape of the liquid bulge after dispensing 3 water droplets (each having a volume 13.3 μl). The liquid spreads along the superhydrophilic tracks, dragging the liquid along the (a) superhydrophobic and (b) hydrophilic axial track. The distance x is determined between the narrowest edge of the track and the vertex of the parabola of the bulge. The white bar at the top denotes 5 mm.

The main objective of the geometry optimization of the design is to obtain a configuration which allows the complete liquid coverage of the amine-functionalized axial track while minimizing the amount of liquid dispensed. Hence, the most important parameter that is necessary to maximize is the distance x of the propagating liquid front along the amine-functionalized track. For larger x, the amount of sample required to ensure coverage of the axial track can be reduced. The following parameters are optimized in this study:

- Superhydrophilic wedge angle α
- Amine-functionalized axial track angle β

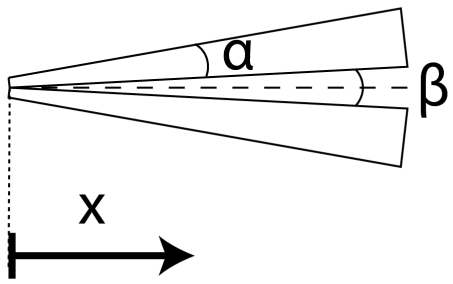

Figure 24: β is the angle of the amine-functionalized axial track, α is the superhydrophilic wedge angle and x is the position of the propagation front of the liquid droplet on the amine-functionalized track. Note that the origin corresponds to the beginning of the track.

The shape of the bulge is also analyzed in similar configuration featuring the same geometry of the previous one: $\alpha = 5°$, $\beta = 6°$ and length of 20 mm (see Figure 24, but the central track, this time, is superhydrophobic (Figure 23-a). Also, as can be seen visually between Figure 23-a and Figure 23-b, the bulge location is dependnent on the wettability of the axial track.

In order to optimize the design, it is necessary to try different configurations by varying the characteristic parameters (*i.e.* wedge angles). Since the shape of the propagating liquid front between the design with the hydrophilic and superhydrophobic axial tracks are very similar (both parabolic), the optimization process is carried out with a design featuring a superhydrophobic axial track. This was done as a proof of concept, due to fabrication time (more time consuming to prototype a design with the amine-functionalized hydrophilic track). For the superhydrophobic axial track case, during sample fabrication, it is only necessary to spray a coating dispersion of TiO_2 and PMC and to create two superhydrophilic tracks under UV by means of a simple photomask. During the optimization process, the test configurations are characterized by different α and β angles (Figure 25). The angle α of the superhydrophilic tracks varies between 2 ° and 7 ° with an increment of 1 °, while the angle of the axial track, β, varies between 6 ° and 10° with an increment of 2 °. It is important to note that the values of β is dictated by considering the surface area of the axial track. Indeed, by considering $\beta = 6°$, $\beta = 8°$, and $\beta = 10°$, the surface areas of the axial track are 20.95, 27.94, and 34.92 mm^2, respectively. These areas are appropriate for a detection region that has to be analyzed under a fluorescence microscope.

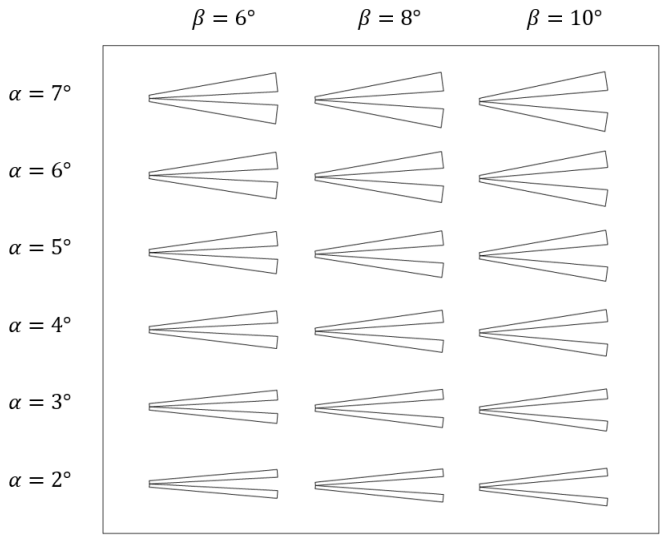

Figure 25: Schematic of the different configurations of design 3 that were evaluated for optimization. They are characterized by a superhydrophilic track angle, α, ranging from 2 ° to 7 ° with an increment of 1 ° and an axial track angle, β, ranging from 6 ° to 10° with an increment of 2 °.

The position of the front, x, is evaluated for all configurations by dispensing three identical water droplets with a dispensing needle, where the average value of x from 4 attempts is calculated. Figure 26 shows the results for the case where optimization is carried out with a superhydrophobic axial, where the position x of the propagating front on the axial track is a function of the superhydrophilic wedge angle α for different β angles.

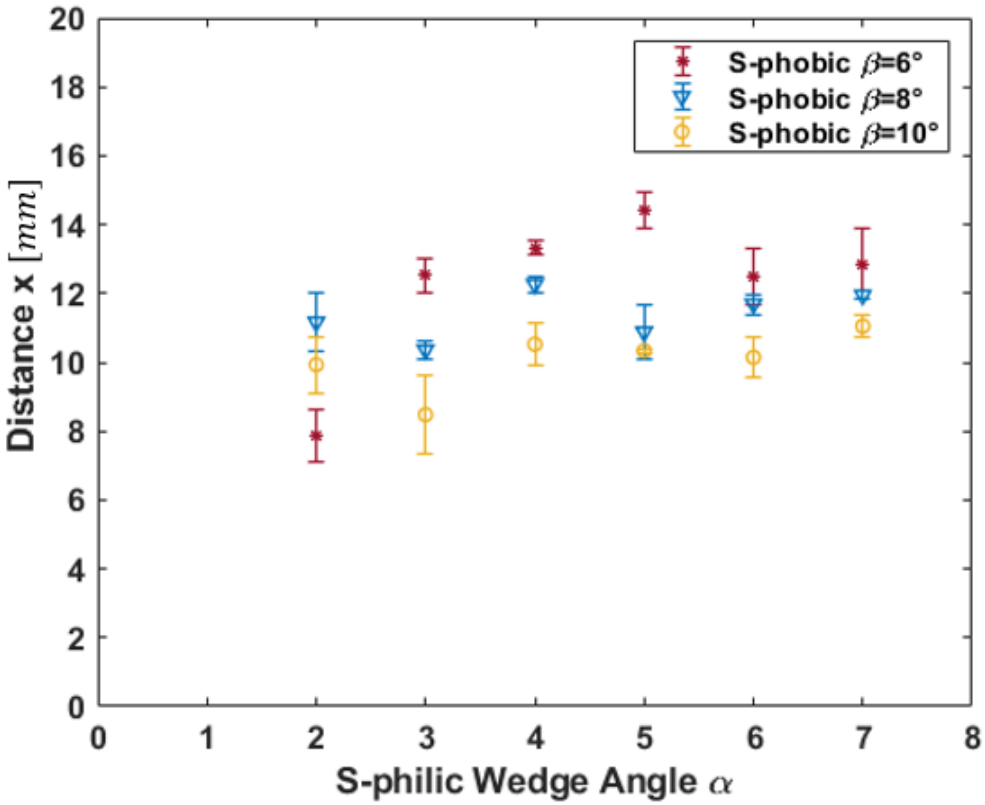

Figure 26: Distance x of the liquid front from the narrowest edge of the track after dispensing 3 droplets over a superhydrophobic axial track. The parameter x is a function of the superhydrophilic track angle α. The length of the error bar is $\pm\sigma$ (standard deviation of 4 attempts).

Figure 26 plot highlights that for larger β, the x position is generally lower. This behavior is explained by noting that by decreasing the angle β, the volume of dispensed liquid (V=13.3 μL) has to spread over a lower surface area, leading to an advanced position of the front. The

maximum value of x is obtained for $\beta = 6°$ and $\alpha = 5°$. This is the best configuration for the design characterized by two superhydrophilic tracks and a superhydrophobic axial track, and this design allows the largest area coverage with the lowest volume dispensed.

Once the transport behavior on different track geometries was known, the position x of the liquid front in the case of interest (amine-functionalized axial track) was then evaluated. The analysis is performed for only few combinations of α and β and the general behavior is extrapolated by comparing these values with the previous ones (Figure 26) obtained by testing the superhydorphobic axial track for all different combinations of angles. The configurations tested for the amine-functionalized axial track are feature the highest β ($\beta = 10°$) and the lowest β ($\beta = 6°$) with α =3 °, 4 °, 5 °, 6 °. The position x is always evaluated by considering the dispensing of three identical liquid droplets ($V_{tot} \approx 39.9$ μL). Figure 27 and Figure 28 compared the results obtained on the silane-functionalized track with the previous ones.

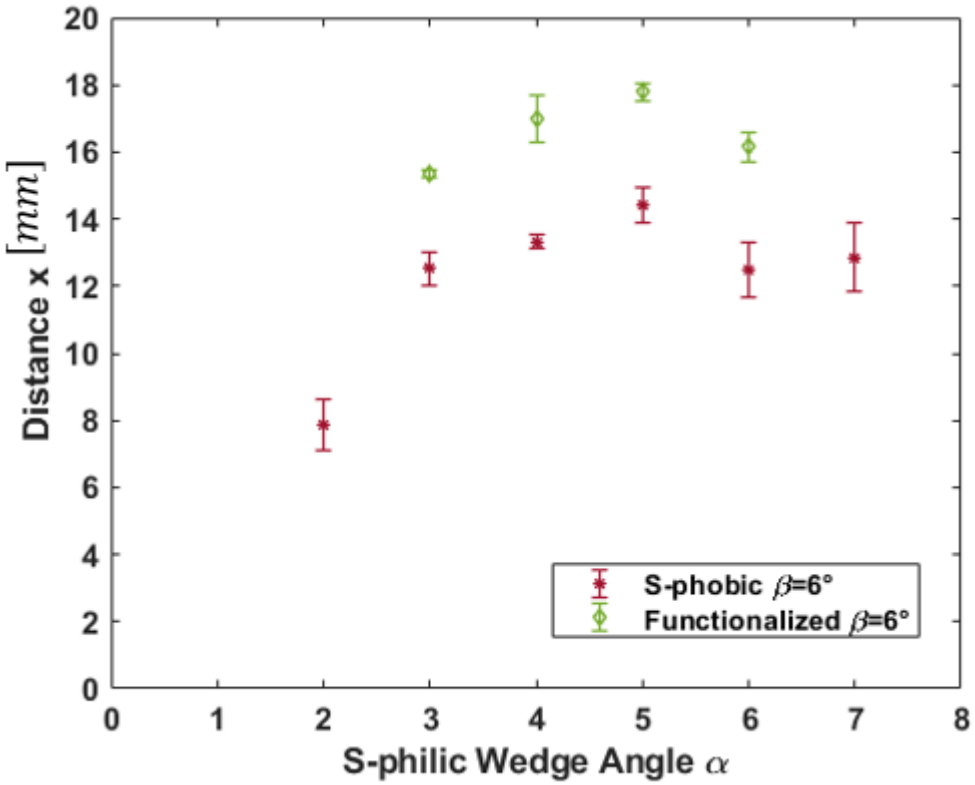

Figure 27: Distance x evaluated for different superhydrophilic angle α along a silane-functionalized and superhydrophobic axial track for $\beta = 6°$. The length of the error bars is $\pm\sigma$ (standard deviation of 4 attempts).

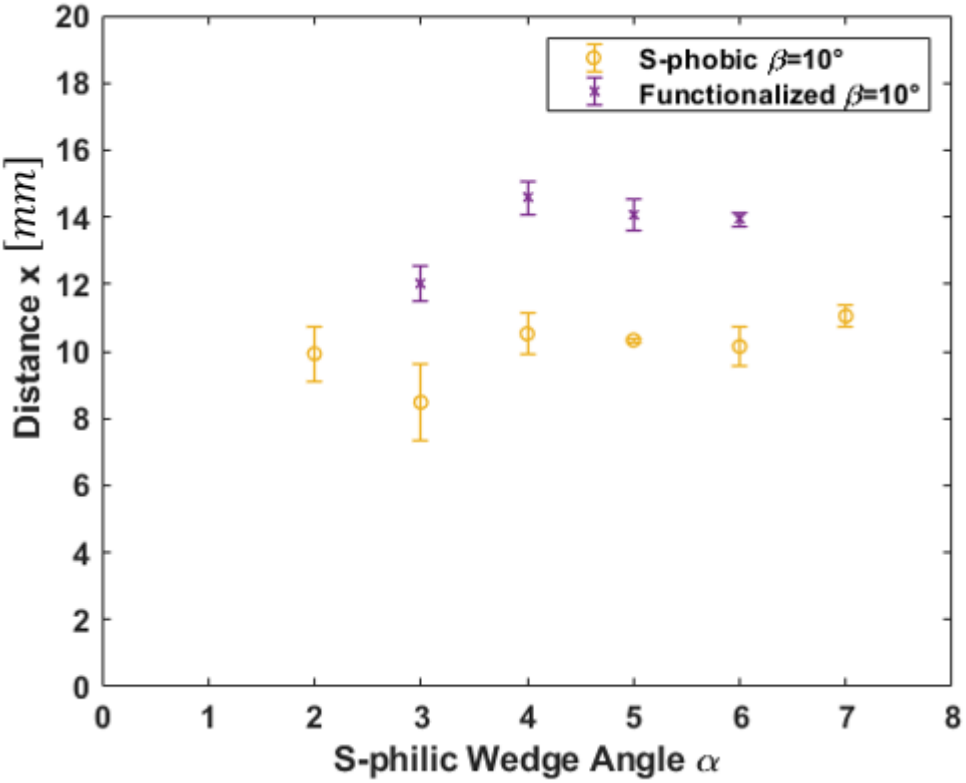

Figure 28: Distance x evaluated for different superhydrophilic angle α along a silane-functionalized and superhydrophobic axial track for $\beta = 10°$. The length of the error bars is $\pm\sigma$ (standard deviation of 4 attempts).

For both cases, the maximum value of x is obtained for a design with $\beta = 6°$ and $\alpha = 5°$ (see Figure 27 and Figure 28). Furthermore, the data trend for the silane-functionalized axial track is very similar to that one obtained for the superhydrophobic track. In the first case (silane-functionalized axial track), the distance x reached by the liquid front increases of approximately

3 mm with respect to the second one. This behavior is explained by analyzing and comparing the final energies of both systems, and this is done through a simple surface energy analysis. Here, all parameters pertaining to the design with the superhydrophobic axial track are indicated by subscript 1, while the design featuring a silane-functionalized axial track is indicated by subscript 2. The control volume considered in both cases is the liquid. Since the volume of liquid dispensed on both tracks is the same ($V_{tot} \approx 39.9$ μL corresponding to the sum of 3 droplets), the initial energies for both systems, $E_{1,initial}$ and $E_{2,initial}$, can be written as:

$$E_{1,initial} = E_{2,initial} = 3\gamma_{LG} 4\pi r^2 \tag{4.1}$$

where r is the radius of each droplet. By applying the conservation of energy:

$$E_{1,initial} = E_{1,final} + E_{d1} \qquad E_{2,initial} = E_{2,final} + E_{d2} \tag{4.2}$$

the following correlation is obtained:

$$E_{1,final} + E_{d1} = E_{2,final} + E_{d2} \tag{4.3}$$

The assumptions to evaluate the final energies of the systems are outlined below:

- The shape of the liquid propagating front is considered to be a line instead of a parabola;

- $A_{LG\uparrow}$ and $A_{LG\downarrow}$ (surface area of the upper and lower liquid-air interface of the fluid) are evaluated by computing the surface area of the trapezoid obtained by projecting $A_{LG\uparrow}$ and $A_{LG\downarrow}$ on the substrate plane.

The final energy is first evaluated for system 1 (the superhydrophobic axial track). Due to the highly non wetting characteristic of the superhydrophobic region, the fluid forms a bridge between the two superhydrophilic tracks. Hence, the liquid formed on the design after deposition features two liquid-gas interfaces: one above and the other underneath (see Figure 29).

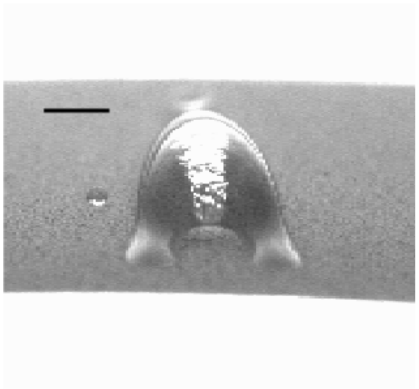

Figure 29: Side view on the widest edge of the track for the desgn which features a superhydrophobic axial track. The fluid forms a liquid bridge between the two superhydrophilic tracks, due to the highly non wetting characteristic of the superhydrophobic region. This “shimmer" seen under the middle of the liquid bulge indicates that there is an air layer between the liquid and the substrate. The black bar at the top denotes 2 mm.

The final energy of the system 1 is computed as:

$$E_{1,final} = \gamma_{LG}\ A_{LG\uparrow 1} + \gamma_{LG}\ A_{LG\downarrow 1} + \gamma_{LS_{s-phillic}}\ A_{LS_{s-philic}1} \tag{4.4}$$

where $A_{LG\uparrow 1}$ and $A_{LG\downarrow 1}$ are the surface area of the liquid cap above and underneath (liquid-

gas interfaces), respectively. $A_{LS_{s-philic}1}$ is the surface area of the superhydrophilic tracks (liquid-solid interface). The surface areas are illustrated in Figure 30 and computed as:

$$A_{LG\uparrow 1} = \frac{2x_1}{\cos\frac{\beta}{2}\cos\frac{\alpha}{2}}\left(b + \frac{x_1\tan\frac{\alpha}{2}}{\cos\frac{\beta}{2}}\right) + \frac{x_1^2\tan\frac{\beta}{2}}{2} \tag{4.5}$$

$$A_{LG\downarrow 1} = \frac{x_1^2\tan\frac{\beta}{2}}{2} \tag{4.6}$$

$$A_{LS_{s-philic}1} = \frac{2x_1}{\cos\frac{\beta}{2}\cos\frac{\alpha}{2}}\left(b + \frac{x_1\tan\frac{\alpha}{2}}{\cos\frac{\beta}{2}}\right) \tag{4.7}$$

where b is the length of the narrowest edge of the superhydrophilic tracks, and x_1 is the position of the propagating front of the liquid on the superhydrophobic track.

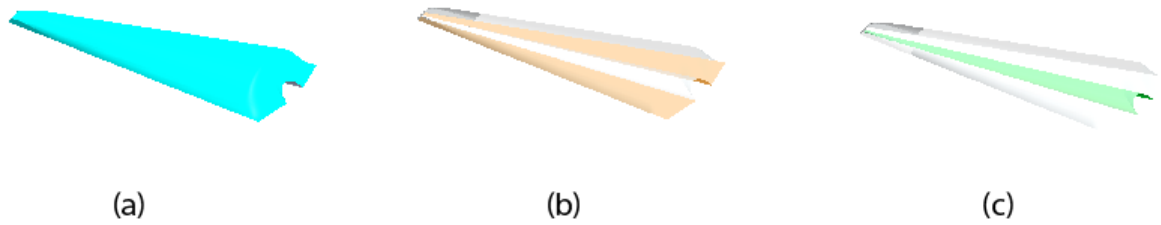

Figure 30: Representation of the surface areas used in the calculation for a design featuring a superhydrophobic axial track: (a) $A_{LG\uparrow 1}$ is the surface area of the liquid cap above (liquid-gas interface), (b) $A_{LS_{s-philic}1}$ is that of the superhydrophilic tracks (liquid-solid interface), and (c) $A_{LG\downarrow 1}$ is that of the liquid cap underneath (liquid-gas interface).

The final energy $E_{1,final}$ for the system is given by:

$$E_{1\,final} = \gamma_{LG}\left(\frac{2x_1}{\cos\frac{\beta}{2}\cos\frac{\alpha}{2}}\left(b + \frac{x_1\tan\frac{\alpha}{2}}{\cos\frac{\beta}{2}}\right) + \frac{x_1^2\tan\frac{\beta}{2}}{2}\right) + \gamma_{LG}\left(\frac{x_1^2\tan\frac{\beta}{2}}{2}\right) + \\ + \gamma_{LS_{s-phillic}}\left(\frac{2x_1}{\cos\frac{\beta}{2}\cos\frac{\alpha}{2}}\left(b + \frac{x_1\tan\frac{\alpha}{2}}{\cos\frac{\beta}{2}}\right)\right) \tag{4.8}$$

By combining the terms x_1 and x_1^2, $E_{1,final}$ is written as:

$$E_{final_1} = x_1\left(\gamma_{LG}\frac{2b}{\cos\frac{\beta}{2}\cos\frac{\alpha}{2}} + \gamma_{LS_{s-phillic}}\frac{2b}{\cos\frac{\beta}{2}\cos\frac{\alpha}{2}}\right) + \\ + x_1^2\left(\gamma_{LG}\frac{2\tan\frac{\alpha}{2}}{\cos^2\frac{\beta}{2}\cos\frac{\alpha}{2}} + \gamma_{LG}\frac{\tan\frac{\beta}{2}}{2} + \gamma_{LG}\frac{\tan\frac{\beta}{2}}{2} + \gamma_{LS_{s-phillic}}\frac{2\tan\frac{\alpha}{2}}{\cos^2\frac{\beta}{2}\cos\frac{\alpha}{2}}\right) \tag{4.9}$$

For system 2, due to the high wettability of the silane-functionalized track, the liquid inherently wets the axial track during the transport, and thus there is no liquid bridge formation (see Figure 31).

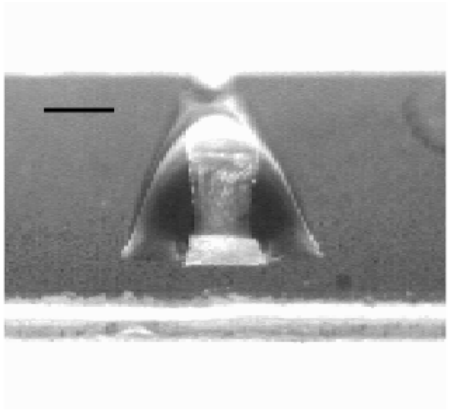

Figure 31: Side view on the widest edge of the track for the design which features an amine-functionalized axial track. The liquid wets the amine-functionalized track during the transport, due to the high wettability of the amine-functionalized track (no formation of the liquid bridge). The black bar at the top denotes 2 mm.

Hence, the final energy of system 2 is computed as:

$$E_{2,final} = \gamma_{LG}\ A_{LG\uparrow 2} + \gamma_{LS_{philic}}\ A_{LS_{philic}2} + \gamma_{LS_{s-phillic}}\ A_{LS_{s-philic}2} \tag{4.10}$$

where $A_{LG\uparrow 2}$ is the surface area of the liquid cap above (liquid-gas interface), $A_{LS_{philic}2}$ is that of the amine-functionalized axial track (liquid-solid interface) and $A_{LS_{s-philic}2}$ is that of the superhydrophilic tracks (liquid-solid interface). The surface areas are illustarted in Figure 32 and computed as:

$$A_{LG\uparrow 2} = \frac{2x_2}{\cos\frac{\beta}{2}\cos\frac{\alpha}{2}}\left(b + \frac{x_2\tan\frac{\alpha}{2}}{\cos\frac{\beta}{2}}\right) + \frac{x_2^2\tan\frac{\beta}{2}}{2} \tag{4.11}$$

$$A_{LS_{philic}2} = \frac{x_2^2\tan\frac{\beta}{2}}{2} \tag{4.12}$$

$$A_{LS_{s-philic}2} = \frac{2x_2}{\cos\frac{\beta}{2}\cos\frac{\alpha}{2}}\left(b + \frac{x_2\tan\frac{\alpha}{2}}{\cos\frac{\beta}{2}}\right) \tag{4.13}$$

where b is defined as above, and x_2 is the position of the propagating front of the liquid on the philic amine-funtionalized track.

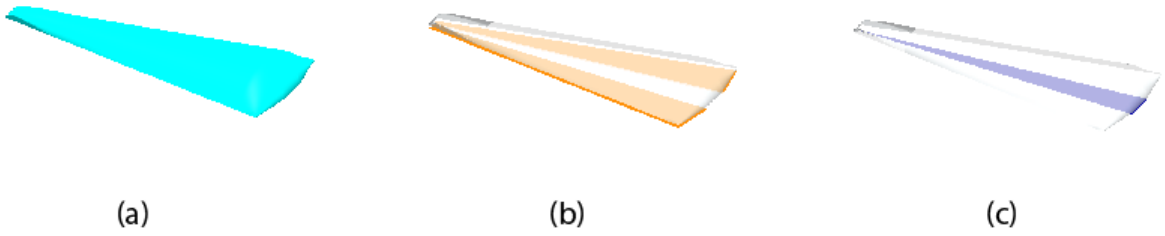

Figure 32: Representation of the surface areas used in the calculation for a design featuring a amine-functionalized axial track: (a) $A_{LG\uparrow 2}$ is the surface area of the liquid cap above (liquid-gas interface), (b) $A_{LS_{s-philic}2}$ is that of the superhydrophilic tracks (liquid-solid interface), and (c) $A_{LS_{philic}2}$ is that of the silane-functionalized axial track (liquid-solid interface).

Thus, the final energy $E_{2,final}$ for the system is given as:

$$E_{2final} = \gamma_{LG}\left(\frac{2x_2}{\cos\frac{\beta}{2}\cos\frac{\alpha}{2}}\left(b + \frac{x_2\tan\frac{\alpha}{2}}{\cos\frac{\beta}{2}}\right) + \frac{x_2^2\tan\frac{\beta}{2}}{2}\right) + \gamma_{LS_{philic}}\left(\frac{x_2^2\tan\frac{\beta}{2}}{2}\right) + \\ + \gamma_{LS_{s-phillic}}\left(\frac{2x_2}{\cos\frac{\beta}{2}\cos\frac{\alpha}{2}}\left(b + \frac{x_2\tan\frac{\alpha}{2}}{\cos\frac{\beta}{2}}\right)\right) \tag{4.14}$$

where by combining the terms x_2 and x_2^2, $E_{2,final}$ can be written as:

$$E_{2final} = x_2\left(\gamma_{LG}\frac{2b}{\cos\frac{\beta}{2}\cos\frac{\alpha}{2}} + \gamma_{LS_{s-phillic}}\frac{2b}{\cos\frac{\beta}{2}\cos\frac{\alpha}{2}}\right) + \\ + x_2^2\left(\gamma_{LG}\frac{2\tan\frac{\alpha}{2}}{\cos^2\frac{\beta}{2}\cos\frac{\alpha}{2}} + \gamma_{LG}\frac{\tan\frac{\beta}{2}}{2} + \gamma_{LS_{philic}}\frac{\tan\frac{\beta}{2}}{2} + \gamma_{LS_{s-phillic}}\frac{2\tan\frac{\alpha}{2}}{\cos^2\frac{\beta}{2}\cos\frac{\alpha}{2}}\right) \tag{4.15}$$

Two coefficients A and B are introduced to simplify the equations:

$$B = \gamma_{LG}\frac{2b}{\cos\frac{\beta}{2}\cos\frac{\alpha}{2}} + \gamma_{LS_{s-phillic}}\frac{2b}{\cos\frac{\beta}{2}\cos\frac{\alpha}{2}} \tag{4.16}$$

$$A = \gamma_{LG}\frac{2\tan\frac{\alpha}{2}}{\cos^2\frac{\beta}{2}\cos\frac{\alpha}{2}} + \gamma_{LG}\frac{\tan\frac{\beta}{2}}{2} + \gamma_{LS_{s-phillic}}\frac{2\tan\frac{\alpha}{2}}{\cos^2\frac{\beta}{2}\cos\frac{\alpha}{2}} \tag{4.17}$$

and by equating the two final energies of systems 1 and 2 in terms of A, B, x_1, x_2, β, γ_{LG}, and $\gamma_{LS_{philic}}$:

$$E_{d1} + B\ x_1 + x_1^2\left(A + \gamma_{LG}\frac{\tan\frac{\beta}{2}}{2}\right) = B\ x_2 + x_2^2\left(A + \gamma_{LS_{philic}}\frac{\tan\frac{\beta}{2}}{2}\right) + E_{d2} \tag{4.18}$$

The dissipation energies for both systems are considered similar. In order to establish the relationship of x_1 with respect to x_2 from Equation 4.18 (liquid propagation fronts for the superhydrophobic and amine-functionlized axial track designs, respectively), it is necessary to evaluate the surface tensions γ_{LG} and $\gamma_{LS_{philic}}$. The value of γ_{LG} (water-air interface in our case) is well-known from literature: $\gamma_{LG} \simeq 72.8\frac{mN}{m}$. On the other hand, $\gamma_{LS_{philic}}$ of the amine-functionalized polycarbonate track has to be evaluated. A method to approximate the surface energy of solids by computing contributions given from dispersion and dipole-hydrogen bonding forces can be used [35]. This approach is based on measurement contact angles of two or more liquids (having known surface tension component). The method is based on the thermodynamic wetting equation, which is expressed in function of four parameters given by the Young's equation:

$$\gamma_{LG}\cos\theta = \gamma_{SG} - \gamma_{SL} - \pi_e \tag{4.19}$$

where γ_{LG}, γ_{SG} and γ_{SL} are the surface energies of liquid-vapour, solid-vapour and solid-liquid respectively, and π_e is the equilibrium pressure of adsorbed vapor of the liquid on the solid. Only the values of γ_{LG} and θ are determined by direct experiments. However, in order to predict the adhesion of polymers, it is essential to determine γ_{SG} and γ_{SL}.

Fowkes [36] suggested that the total surface free energy is given by the sum of different intermolecular forces at the surface interface (attractive forces). Thus, the surface free energy of the liquid and of the surface could be written as:

$$\gamma_{LG} = \gamma_L^d + \gamma_L^p \tag{4.20}$$

$$\gamma_{SG} = \gamma_S^d + \gamma_S^p \tag{4.21}$$

where the indeces d and p refer to the dispersion and hydrogen bonding (*i.e.* polar) force components. The use of the more general index S instead of SG assumes that the vapor pressure of the solid is negligible. Furthermore, it is assumed that $\pi_e = 0$ and

$$\gamma_{SL} = \gamma_{SG} + \gamma_{LG} - 2\sqrt{\gamma_S^d \gamma_L^d} - 2\sqrt{\gamma_S^p \gamma_L^p} \tag{4.22}$$

By substituting Equation 4.22 in Equation 4.19:

$$1 + \cos\theta = 2\sqrt{\gamma_S^d}\left(\frac{\sqrt{\gamma_L^d}}{\gamma_{LG}}\right) + 2\sqrt{\gamma_S^p}\left(\frac{\sqrt{\gamma_L^p}}{\gamma_{LG}}\right) \tag{4.23}$$

The above equation can be rewritten as:

$$\frac{\gamma_{LG}(1+\cos\theta)}{2\sqrt{\gamma_L^d}} = \sqrt{\gamma_S^p}\left(\sqrt{\frac{\gamma_L^p}{\gamma_L^d}}\right) + \sqrt{\gamma_S^d} \tag{4.24}$$

Equation 4.24 corresponds to the equation of a straight line:

$$y = mx + b \tag{4.25}$$

To determine the solid-air surface energy of the silane-functionalized track, water and ethylene glycol are used as the two probe liquids and their contact angles are measured, which are equal to 66.88°± 2.04°and 38.82°± 3.92°, respectively (represented in Figure 33). Furthermore, the values γ_L^d, γ_L^p and γ_{LV} are known for both liquids [35].

TABLE II: CHARACTERISTIC VALUES OF θ, γ_L^d, γ_L^p AND γ_{LV} OF WATER AND ETHYLENE GLYCOL

	Water	Ethylene Glycol
θ	66 °	38 °
$\gamma_L^d \ \frac{mN}{m}$	21.8	29
$\gamma_L^p \ \frac{mN}{m}$	51	19
$\gamma_{LG} \ \frac{mN}{m}$	72.8	48

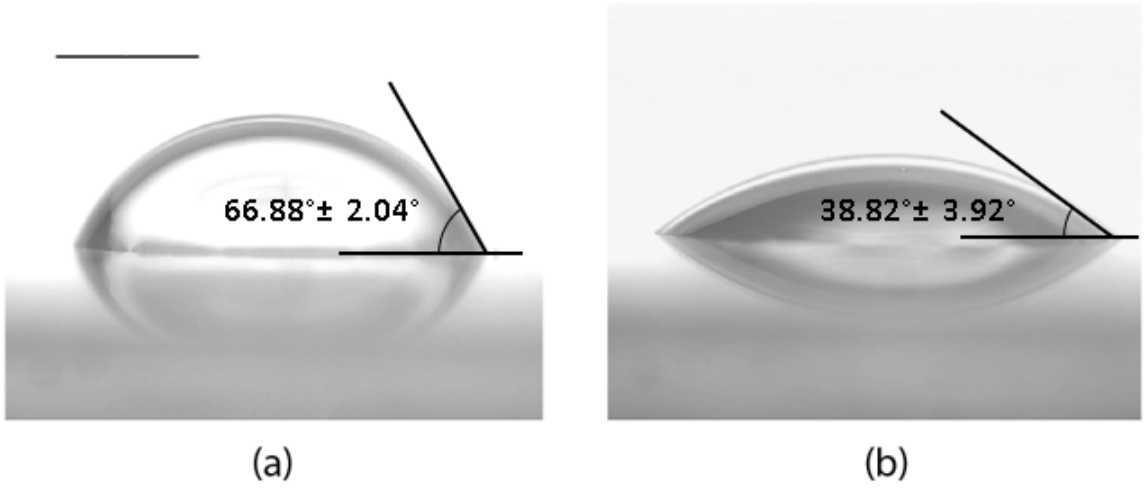

Figure 33: Static contact angles on amine-functionalized substrate for (a) water and (b) ethylene glycol droplets. The black bar at the top denotes denotes 1 mm.

By substituting the known values of Table II into Equation 4.24, a system of two equations with two unknowns (γ_S^d and γ_S^p) is obtained. The system is solved by calculating the slope m and the intersection b of the straight line with the y axis (Figure 34).

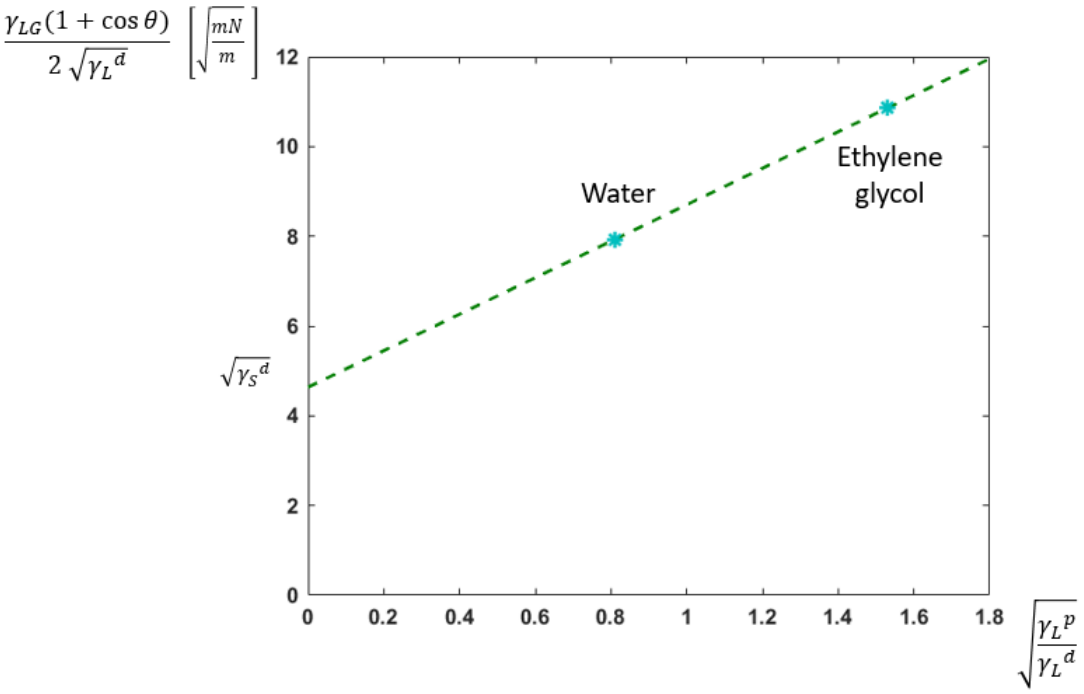

Figure 34: Straight line that describes Equation 4.24. The two points represented on the plot are the values corresponding to water and ethylene glycol. The slope of the straight line and its intersection with the y axis are respectively $\sqrt{\gamma_S^p}$ and $\sqrt{\gamma_S^d}$.

By knowing the value of m and b, γ_S^d, γ_S^p are computed ($\gamma_S^d \approx 21.50\frac{mN}{m}$, $\gamma_S^p \approx 16.50\frac{mN}{m}$). The sum of these two contributions (dispersion and hydrogen adhesion forces) gives a reasonable approximation of the total solid surface energy: $\gamma_{SG} \approx 38\frac{mN}{m}$. The surface tension solid-liquid for the amine-functionalized surface is computed with Young's equation: $\gamma_{LS_{philic}} \approx 7.23\frac{mN}{m}$.

Since $\gamma_{LG} > \gamma_{LS_{philic}}$, Equation 4.18 is satisfied only if $x_2 > x_1$. Therefore, the liquid front has to spread further in the hydrophilic amine-functionalized axial track. This energy analysis approach then justifies the behavior observed in Figure 27 and Figure 28.

4.3 Standard Curve

Once the working mechanism and the optimization of the design was analyzed, we could begin testing protein detection efficacy of the device. The BCA allows the determination of total concentration of proteins in a solution (generally ranges from 0.5 μg/mL to 2 mg/mL). In this method, the total concentration of proteins is expressed by a color change of the BCA reagent from green to purple with a color intensity proportional to the concentration. To estimate the protein concentration of an unknown sample, a standard curve characteristic of the proteins to be analyzed needs to be used. The standard curve is a graph used as a quantitative research technique and it is represented by making several dilutions of one known concentration of the proteins. The data of these concentrations are plotted as a function of an assay measurable, which is generally represented by the light absorbance of the reagent which is usually evaluated by means of spectrometer. Subsequently, the concentration of unknown samples is evaluated by interpolation of points that belong to that generated standard curve. Thus, to interpret the

absorbance of the unknown substance, it is necessary to locate the measurement on the Y-axis (light absorbance) and to follow a line to intersect the standard curve. The corresponding value on the X-axis coincides to the concentration of antigens in the unknown sample. Typically, a standard curve has a sigmoidal behavior in which the greater is the absorbance, the higher is the protein concentration.

In order to construct the standard curve in this work, the followed procedure is performed:

- The device is made by patterning a silane-functionalized axial track located between two symmetric superhydrophilic tracks, where the axial and superhydrophilic tracks are laid on a superhydrophobic background.
- Five samples with varying concentration of proteins (BSA) are prepared (0.2 mg/mL, 0.4 mg/mL, 0.6 mg/mL, 0.8 mg/mL, and 1 mg/mL).
- 80 μL of each solution made in the previous step are then dispensed on five different tracks (see Figure 35-a). Thus, on each of the five substrates there is a solution with a different concentration of proteins. Afterward, the five substrates (with the liquid on the tracks) are incubated for 1 hour at 37 °C.
- The tracks are washed 3 times, each with 2 mL of DIW (via pipetting) in order to remove all the unbound proteins (Figure 35-b). In particular, the water is dispensed at the narrowest edge of the track and it is transported to the end of the track, where a tissue (Kimtech Science™ Kimwipes™) soaks up the liquid transported (DI water + unbound proteins). At each washing the tissue is changed and other 2 mL of DIW is dispensed in a similar.

- The working reagent is prepared by mixing 50 parts of BCA reagent A with 1 part of BCA reagent B (50:1, Reagent A,B). The color of the solution is green at this point. 160 μL of this solution is dispensed at the beginning of the track and transported to cover all the transport and detection region of each substrate(Figure 37-a).
- The five substrates with the BCA reagent (different concentrations between substrates) are incubated for 30 minutes at 37 °C. A color change is produced (green to purple) if BSA proteins are present on the substrate. The intensity of the color is proportional to the concentration of the antigens in the solution (Figure 37-b).
- After 30 min of incubation, 100 μL of solution are removed from each substrate by means of a pipette and dispensed onto the well of the microplates. Thus, these five wells of the microplates are filled by an known different concentration of proteins.
- The microplates are positioned onto a plate reader which determines the absorbance of each unknown solution. The absorbance frequency is set to the maximum value (A_{max}) of the BCA reagent (562 nm).

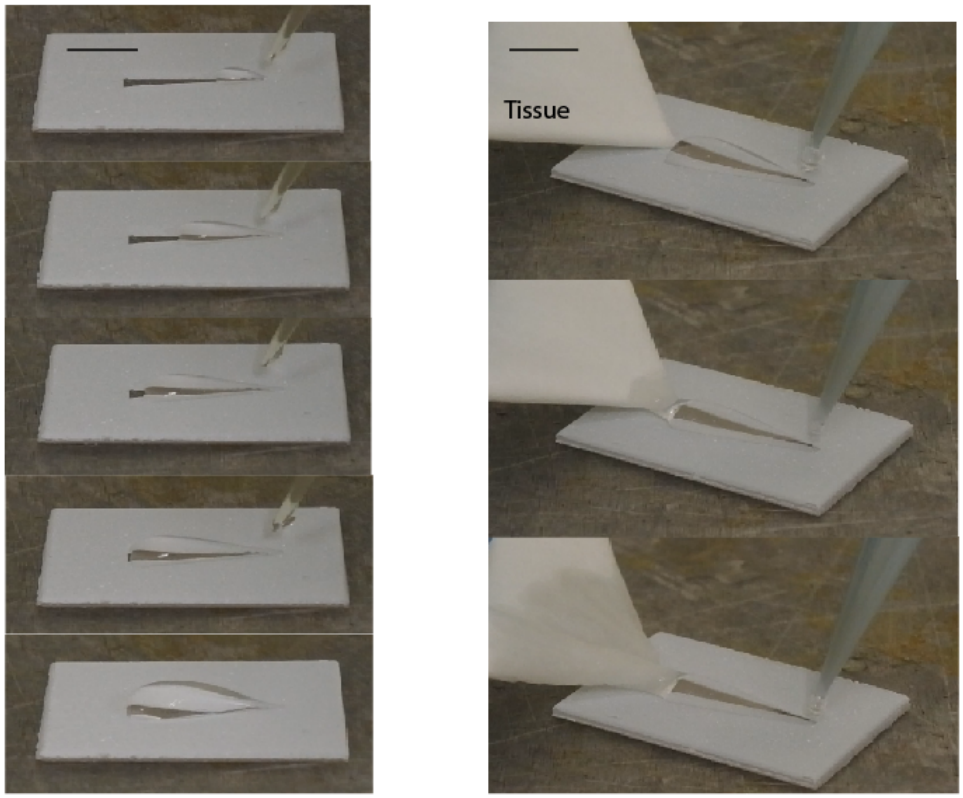

Figure 35: (a) Transport of BSA proteins and DI water. The total dispensing volume is 80 μL. (B) Tracks are washed three times to remove unbound proteins (each with 2 mL of DI water) and a tissue at the end of the tracks soaks up the liquid.

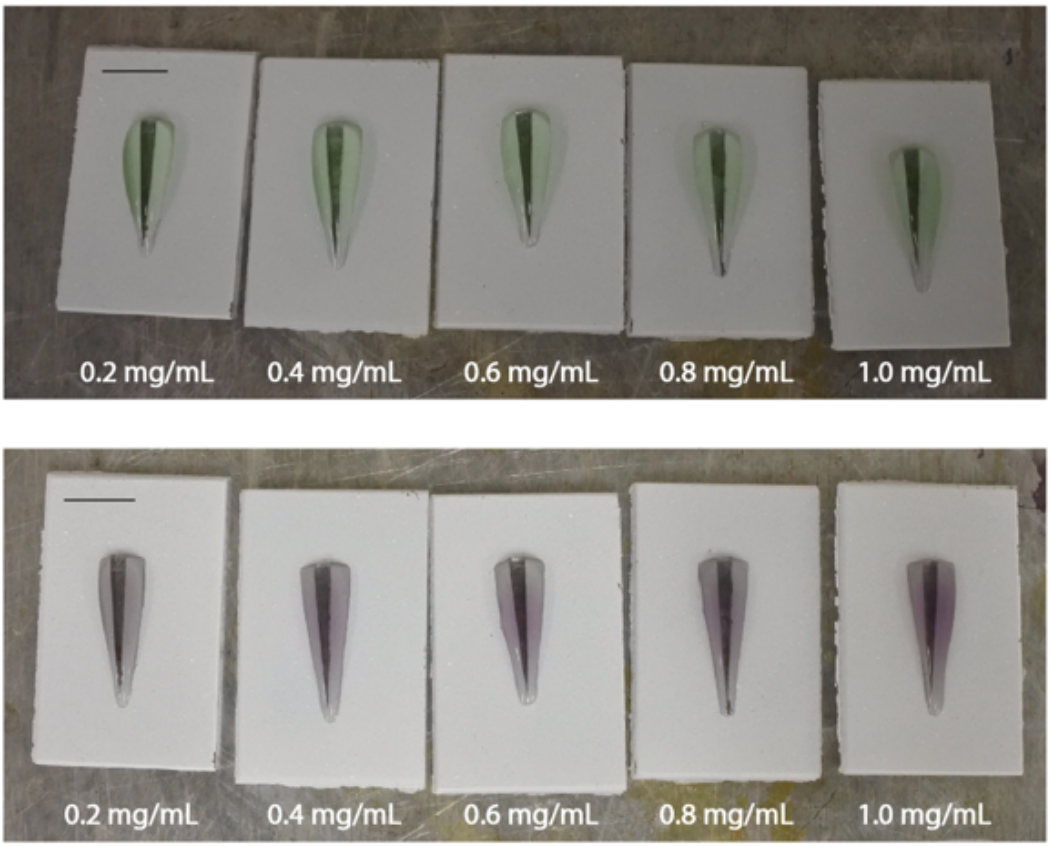

Figure 36: (a) 160 μL of green BCA reagent is dispensed at the beginning of the track and transported to cover all the transport and detection region of each substrate. (b) The color of the reagent changes due to the presence of the proteins and its intensity is proportional to the concentration. Notice that as the concentration of added BSA bound to the axial track increases, so does to intensity of the purple color.

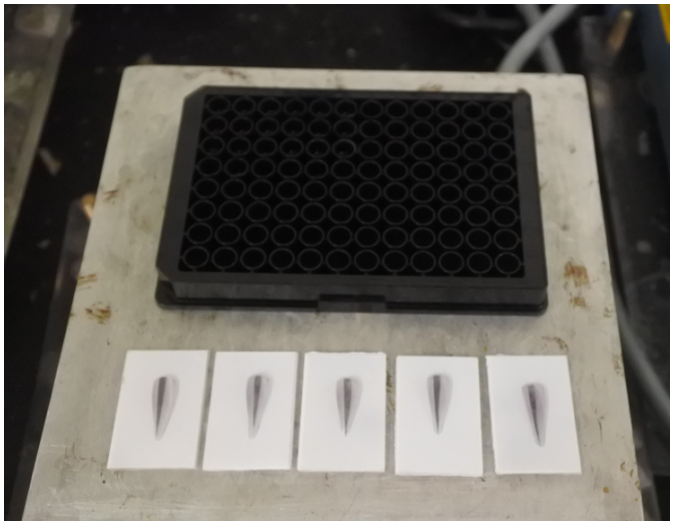

Figure 37: 100 μL of solution are removed from each substrate by means of a pipette and dispensed onto the well of the microplates.

The standard curve is generated by graphing the absorbance for each sample obtained from the above steps (y-axis) as a function of the standard concentration of proteins (x-axis) (Figure 38).

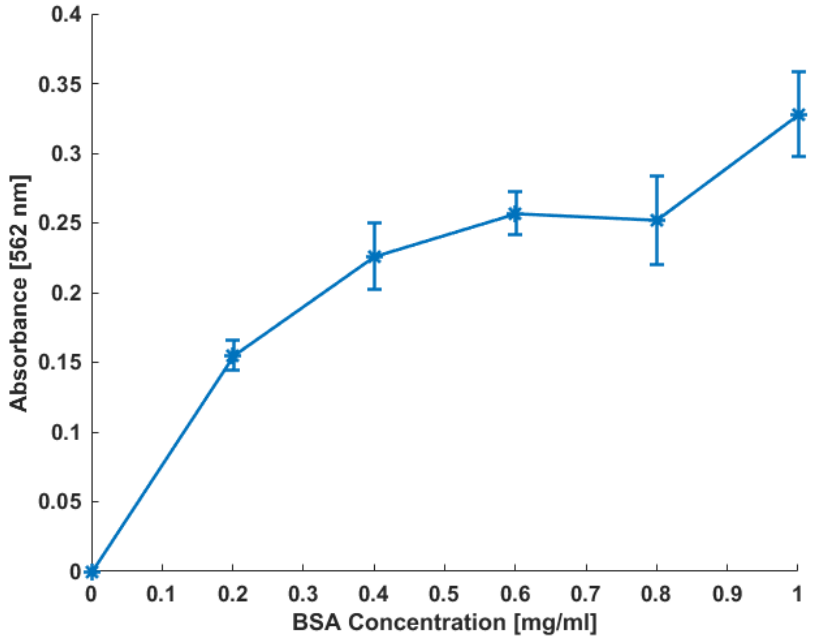

Figure 38: Standard curve for BCA assay. The absorbance (562 nm) is plotted in function of the BSA concentration.

The results expressed in the graph showed the expected behavior characteristic of a standard curve: the higher is the absorbance, the higher is the concentration of the proteins.

CHAPTER 5

CONCLUSION AND FUTURE WORK

In the present work, a device for the detection of proteins has been developed. The detection technique used to quantify the concentration of proteins is the bicinchoninic acid (BCA) assay. A solution of proteins (bovine serum albumin, or BSA) and DI water is transported on dedicated wedge-shaped transport tracks and the solution ultimately wets a detection region. Here, some BSA proteins attach to the surface, which has been previously functionalized with an aminosilane (APTES). Silane functionalization is necessary to immobilize BSA proteins to the surface of the detection zone. After transporting the BSA solution, all other unbound proteins are removed by performing several washings with DI water. Afterward, BCA reagent is added to the detection zone and its color changes from green to purple if BSA proteins are present on the surface. The color intensity is directly proportional to the concentration of antigens. Polycarbonate was used as the device since this material allows for a transparent detection zone, a property which is essential for the quantification of the color intensity under a fluorescence microscope.

The transport region of the device is made by patterning a specific spatial wettability contrast (wedge-shaped), which allows a spontaneous pumpless transport of a liquid. Different designs are considered, and the most suitable design for the purpose of this work relies on a silane-functionalized axial track located between two symmetric superhydrophilic tracks, where

the axial and superhydrophilic tracks are laid on a superhydrophobic background. The geometry of this design (*e.g.* track angles) is optimized in order to obtain the complete coverage of the detection zone, while minimizing the volume of liquid needed for complete coverage. The optimal angles for the s-philic tracks, α, and silane-functionalized axial track, β, are $\alpha = 5°$, and $\beta = 6°$, respectively.

After design optimization, a “standard curve" is generated in order to make evaluations of an unknown concentration of proteins dispensed on the track possible. A standard curve is a graph representing BCA reagent absorbance as a function of protein concentration. The standard curve is generated by analyzing the color intensity produced by the BCA reagent when it reacted with a known concentration of BSA proteins. The curve is generally sigmoidal: higher intensity generally correlated with higher protein concentration.

Since the results obtained in this work successfully showed the expected behavior characteristic of a standard curve, the proposed device should be employed in the analysis of human skin oil. The BCA technique (employed in this work) has been used only as a proof of concept for the enzyme-linked immunosorbent assay (ELISA). This was done as a preliminary step due to the complexity, sample fabrication time, and high cost of samples associated with variations of the ELISA technique. The ELISA method generally consists on the immobilization of an antigen on a solid surface, that subsequently pairs with an antibody linked to an enzyme. Detection is achieved by making the conjugated enzyme react with a substrate to produce a fluorescence,

and the fluorescence is then analyzed under the inverted fluorescence microscope. However, there are different type of ELISA techniques: direct, indirect, sandwich, or competitive. The most effective and common type is the sandwich assay (Figure 39), whose name is due to the fact that the protein of interest is bonded between two primary antibodies (A and C), where one is immobilized by a functionalized surface and the other one is linked to the protein (B). The detection antibody (D), connected to the primary antibody (C), is linked to an enzyme (E) which reacts with the substrate (F) to produce the fluorescence. This type of ELISA is the optimal solution for the detection of proteins contained in the human skin oil because of its improved robustness and sensitivity compared to the other methods. Thus, it could be adopted for the future implementation of the device.

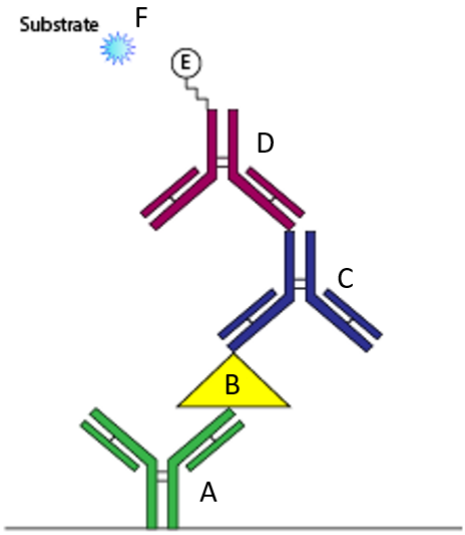

Figure 39: Relevant steps of ELISA Sandwich: the primary antibody (A) is immobilized by the functionalized surface. The protein of interest (B) is bonded between two primary antibodies (A and C). Then, the detection antibody (D), connected to the primary antibody (C), is linked to an enzyme (E) which reacts with the substrate (F) to produce the fluorescence.

ELISA is typically performed using a kit with 96-well plates in polystyrene, which passively bind antibodies or proteins. The bottom surface of the well is functionalized, and consequently it is able to immobilize antibodies or proteins (depending on the procedure). In this case, instead of performing the ELISA on microplates, the proposed open-surface device with a specific wettability patterning and a detection functionalized region has to be employed.

The ELISA assay provides two different type of outcome:

- Quantitative: A known concentration of antigen is used to generate a *standard curve*: a graph representing the protein concentration as a function of the optical fluorescence (sigmoidal curve). By analyzing the fluorescence produced by an unknown sample, the concentration of proteins on this sample can be determined with linear interpolation between two points on the standard curve. If the ELISA is performed with well microplates, the fluorescence is determined by using a typical ELISA plate reader. On the other hand, if the microplates are not used, different techniques, such as the fluorescence microscope can be used.
- Qualitative: ELISA results indicate only whether an antigen is present in the specific sample or not. This can be done by comparing the given sample fluorescence with the one produced by a sample in which that protein is not present.

Furthermore, the ELISA techniques harness the specificity of proteins. In nature, there are different types of antigens and antibodies, and each antibody is only able to bind to its respective antigen, where the chemical structure of the antibody determines the specificity of the binding mechanism. Thus, by using a specific antibody during the ELISA assay, it is possible to select and detect the concentration of only one type of antigen. The result is a particular antigen-antibody complex which allows one to evaluate the concentration of that antigen within the complex. On the other hand, the BCA technique shown in this work does not harness this specificity, but rather detects the presence of any proteins contained in the solution. Since human skin oil contains different types of detectable proteins, the ELISA technique must be

employed to identify the quantity of each kind of antigens.

Moreover, all kind of proteins contained in human skin oil could be potentially detected simultaneously by adopting a radially outward arrangement of divergent tracks to create droplets splitting (Figure 41) device. A droplet of solvent could potentially be deposited onto a central spot, where a membrane previously rubbed on the skin is positioned. The droplet of solvent should extract the proteins present in the membrane, and the droplet can split (equal volumes) among the tracks. The ELISA may be performed by selecting a specific antibody for each track. In that way, it could be possible to evaluate the concentration of a specific protein on each track.

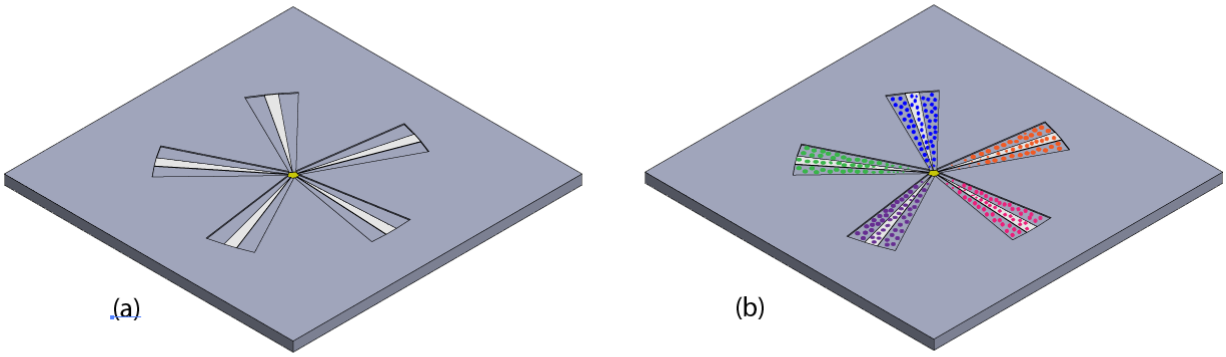

Figure 40: (a) Radially outward arrangment of divergent tracks with the sample membrane positioned at the centre. (b) Each track presents specific antibody (represented with different colors) which binds to its respective antigen.

APPENDICES

Appendix A

AUTHORIZATION FOR IMAGE USED IN FIGURE 6

Royal Society of Chemistry LICENSE TERMS AND CONDITIONS

Apr 15, 2019

This is a License Agreement between helene della monica ("You") and Royal Society of Chemistry ("Royal Society of Chemistry") provided by Copyright Clearance Center ("CCC"). The license consists of your order details, the terms and conditions provided by Royal Society of Chemistry, and the payment terms and conditions.

All payments must be made in full to CCC. For payment instructions, please see information listed at the bottom of this form.

License Number	4564990532416
License date	Apr 09, 2019
Licensed content publisher	Royal Society of Chemistry
Licensed content title	Lab on a chip
Licensed content date	Jan 1, 2001
Type of Use	Thesis/Dissertation
Requestor type	Academic institution
Format	Electronic
Portion	chart/graph/table/figure
Number of charts/graphs/tables/figures	1
The requesting person/organization is:	Helene Della Monica
Title or numeric reference of the portion(s)	Pumpless open-surface microfluidic device for proteins detection
Title of the article or chapter the portion is from	N/A
Editor of portion(s)	N/A
Author of portion(s)	N/A
Volume of serial or monograph.	N/A
Page range of the portion	60
Publication date of portion	05/10/2019
Rights for	Main product
Duration of use	Current edition and up to 5 years
Creation of copies for the disabled	no
With minor editing privileges	no
For distribution to	Worldwide
In the following language(s)	Original language of publication

With incidental promotional use	no
The lifetime unit quantity of new product	Up to 499
Title	Pumpless open-surface microfluidic device for proteins detection
Institution name	university of illinois of chicago
Expected presentation date	May 2019
Total (may include CCC user fee)	0.00 USD

Appendix B

BIOACTIVITY OF A SUPERHYDROPHILIC TRACK COMPOSED BY TITANIUM DIOXIDE ANATASE EXPOSED TO UV LIGHT

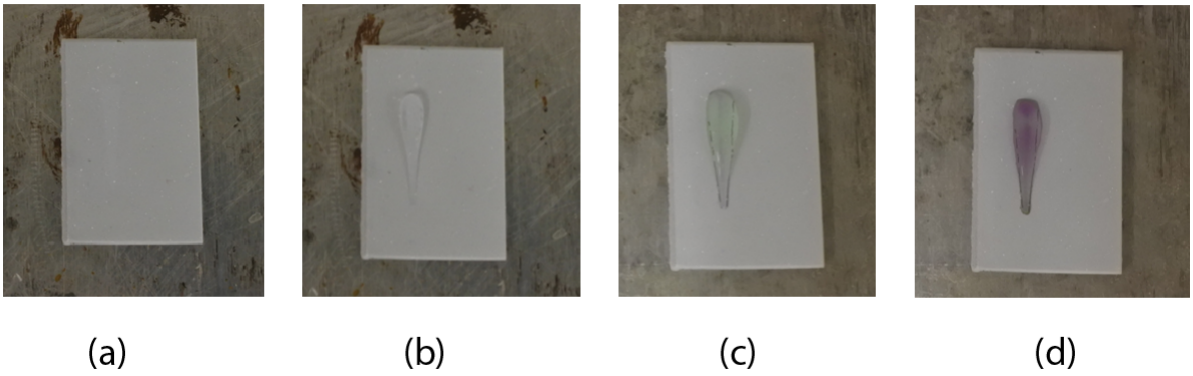

Figure 41: (a) A substrate is made by patterning a superhydrophilic track (which is made of titanium dioxide anatase exposed under UV light) laid in a superhydrophobic region. (b) A solution of BSA and DI water is dispensed on the track and incubated for 1 hour at 37 ° C. The track is washed 5 times. (c) The BCA working reagent is dispensed and incubated for 30 min at 37 ° C. (d) The reagent changes color from green to purple, highlighting the capability of the treated TiO_2 under UV to adsorb proteins.

CITED LITERATURE

1. De Gennes, P.-G., Brochard-Wyart, F., and Quéré, D.: Capillarity and wetting phenomena: drops, bubbles, pearls, waves. Springer Science & Business Media, 2013.

2. Herold, K. E. and Rasooly, A.: Lab on a Chip Technology: Fabrication and microfluidics, volume 1. Horizon Scientific Press, 2009.

3. Issadore, D. and Westervelt, R. M.: Point-of-care Diagnostics on a Chip. Springer Science & Business Media, 2013.

4. Chin, C. D., Linder, V., and Sia, S. K.: Lab-on-a-chip devices for global health: Past studies and future opportunities. Lab on a Chip, 7(1):41–57, 2007.

5. Usdin, M., Guillerm, M., and Calmy, A.: Patient needs and point-of-care requirements for hiv load testing in resource-limited settings. Journal of infectious diseases, 2010.

6. Geschke, O., Klank, H., and Telleman, P.: Microsystem Engineering of Lab-on-a-chip Devices. John Wiley & Sons, 2004.

7. Costa, M., Veigas, B., Jacob, J., Santos, D., Gomes, J., Baptista, P., Martins, R., Inácio, J., and Fortunato, E.: A low cost, safe, disposable, rapid and self-sustainable paper-based platform for diagnostic testing: lab-on-paper. Nanotechnology, 25(9):094006, 2014.

8. Daw, R. and Finkelstein, J.: Lab on a chip. Nature, 442(7101):367, 2006.

9. Kong, D. S., Thorsen, T. A., Babb, J., Wick, S. T., Gam, J. J., Weiss, R., and Carr, P. A.: Open-source, community-driven microfluidics with metafluidics. Nature biotechnology, 35(6):523, 2017.

10. Cong, H., Xu, X., Yu, B., Liu, H., and Yuan, H.: Fabrication of anti-protein-fouling poly (ethylene glycol) microfluidic chip electrophoresis by sandwich photolithography. Biomicrofluidics, 10(4):044106, 2016.

11. Hourtane, V., Bodiguel, H., and Colin, A.: Dense bubble traffic in microfluidic loops: Selection rules and clogging. Physical Review E, 93(3):032607, 2016.

CITED LITERATURE (continued)

12. Sen, U., Chatterjee, S., Ganguly, R., Dodge, R., Yu, L., and Megaridis, C. M.: Scaling laws in directional spreading of droplets on wettability-confined diverging tracks. Langmuir, 34(5):1899–1907, 2018.

13. Lv, C. and Hao, P.: Driving droplet by scale effect on microstructured hydrophobic surfaces. Langmuir, 28(49):16958–16965, 2012.

14. Bliznyuk, O., Jansen, H. P., Kooij, E. S., Zandvliet, H. J., and Poelsema, B.: Smart design of stripe-patterned gradient surfaces to control droplet motion. Langmuir, 27(17):11238–11245, 2011.

15. Dos Santos, F. D. and Ondarcuhu, T.: Free-running droplets. Physical Review Letters, 75(16):2972, 1995.

16. Chaudhury, M. K. and Whitesides, G. M.: How to make water run uphill. Science, 256(5063):1539–1541, 1992.

17. Chakraborty, M., Ghosh, U. U., Chakraborty, S., and DasGupta, S.: Thermally enhanced self-propelled droplet motion on gradient surfaces. Rsc Advances, 5(56):45266–45275, 2015.

18. Ichimura, K., Oh, S.-K., and Nakagawa, M.: Light-driven motion of liquids on a photoresponsive surface. Science, 288(5471):1624–1626, 2000.

19. Zhao, Y., Liu, F., and Chen, C.-H.: Thermocapillary actuation of binary drops on solid surfaces. Applied Physics Letters, 99(10):104101, 2011.

20. Kooij, E. S., Jansen, H., Bliznyuk, O., Poelsema, B., and Zandvliet, H. J.: Directional wetting on chemically patterned substrates. Colloids and surfaces A: Physicochemical and engineering aspects, 413:328–333, 2012.

21. Yang, J.-T., Yang, Z.-H., Chen, C.-Y., and Yao, D.-J.: Conversion of surface energy and manipulation of a single droplet across micropatterned surfaces. Langmuir, 24(17):9889–9897, 2008.

22. Ghosh, A., Ganguly, R., Schutzius, T. M., and Megaridis, C. M.: Wettability patterning for high-rate, pumpless fluid transport on open, non-planar microfluidic platforms. Lab on a Chip, 14(9):1538–1550, 2014.

CITED LITERATURE (continued)

23. Brinkmann, M. and Lipowsky, R.: Wetting morphologies on substrates with striped surface domains. Journal of applied physics, 92(8):4296–4306, 2002.

24. Teoh, S. H.: Engineering materials for biomedical applications, volume 1. World scientific, 2004.

25. Dixit, C.: Surface modification and conjugation strategies for bioassay/biomaterial applications. Doctoral dissertation, Dublin City University, 2012.

26. Poncin-Epaillard, F., Vrlinic, T., Debarnot, D., Mozetic, M., Coudreuse, A., Legeay, G., El Moualij, B., and Zorzi, W.: Surface treatment of polymeric materials controlling the adhesion of biomolecules. Journal of functional biomaterials, 3(3):528–543, 2012.

27. Ansari, A., Patel, R., Schultheis, K., Naumovski, V., and Imoukhuede, P.: A method of targeted cell isolation via glass surface functionalization. Journal of visualized experiments: JoVE, (115), 2016.

28. Subramanian, R. S., Moumen, N., and McLaughlin, J. B.: Motion of a drop on a solid surface due to a wettability gradient. Langmuir, 21(25):11844–11849, 2005.

29. Xing, S., Harake, R. S., and Pan, T.: Droplet-driven transports on superhydrophobic-patterned surface microfluidics. Lab on a Chip, 11(21):3642–3648, 2011.

30. Morrissette, J. M., Mahapatra, P. S., Ghosh, A., Ganguly, R., and Megaridis, C. M.: Rapid, self-driven liquid mixing on open-surface microfluidic platforms. Scientific reports, 7(1):1800, 2017.

31. Att, W., Hori, N., Iwasa, F., Yamada, M., Ueno, T., and Ogawa, T.: The effect of uv-photofunctionalization on the time-related bioactivity of titanium and chromium–cobalt alloys. Biomaterials, 30(26):4268–4276, 2009.

32. Hori, N., Ueno, T., Minamikawa, H., Iwasa, F., Yoshino, F., Kimoto, K., Lee, M. C.-I., and Ogawa, T.: Electrostatic control of protein adsorption on uv-photofunctionalized titanium. Acta biomaterialia, 6(10):4175–4180, 2010.

33. Lorenzetti, M., Bernardini, G., Luxbacher, T., Santucci, A., Kobe, S., and Novak, S.: Surface properties of nanocrystalline tio2 coatings in relation to the in vitro plasma protein adsorption. Biomedical Materials, 10(4):045012, 2015.

CITED LITERATURE (continued)

34. Gao, Y., Liu, Y., Zhou, L., Guo, Z., Rong, M., Liu, X., Lai, C., and Ding, X.: The effects of different wavelength uv photofunctionalization on micro-arc oxidized titanium. PLoS One, 8(7):e68086, 2013.

35. Owens, D. K. and Wendt, R.: Estimation of the surface free energy of polymers. Journal of applied polymer science, 13(8):1741–1747, 1969.

36. Fowkes, F. M.: Attractive forces at interfaces. Industrial & Engineering Chemistry, 56(12):40–52, 1964.

37. Knuth, D. E.: The TEX Book. Reading, Massachusetts, Addison-Wesley, 1984. Reprinted as Vol. A of *Computers & Typesetting*, 1986.

38. Knuth, D. E.: TEX: The Program, volume B of Computers & Typesetting. Reading, Massachusetts, Addison-Wesley, 1986.

39. Knuth, D. E.: The WEB system for structured documentation, version 2.3. Technical Report STAN-CS-83-980, Computer Science Department, Stanford University, Stanford, California, September 1983.

40. Knuth, D. E.: Literate programming. The Computer Journal, 27(2):97–111, May 1984.

41. Knuth, D. E.: A torture test for TEX, version 1.3. Technical Report STAN-CS-84-1027, Computer Science Department, Stanford University, Stanford, California, November 1984.

42. Furuta, R. K. and MacKay, P. A.: Two TEX implementations for the IBM PC. Dr. Dobb's Journal, 10(9):80–91, September 1985.

43. Désarménien, J.: How to run TEX in french. Technical Report SATN-CS-1013, Computer Science Department, Stanford University, Stanford, California, August 1984.

44. Samuel, A. L.: First grade TEX: A beginner's TEX manual. Technical Report SATN-CS-83-985, Computer Science Department, Stanford University, Stanford, California, November 1983.

45. Lamport, L.: LATEX: A Document Preparation System. User's Guide and Reference Manual. Reading, Massachusetts, Addison-Wesley, 1986.

46. Spivak, M. D.: The Joy of TEX. American Mathematical Society, 1985.

CITED LITERATURE (continued)

47. Patashnik, O.: BibTEXing. Computer Science Department, Stanford University, Stanford, California, January 1988. Available in the BibTEX release.

48. Patashnik, O.: Designing BibTEX Styles. Computer Science Department, Stanford University, January 1988.

49. Fuchs, D.: The format of TEX's DVI files version 1. TUGboat, 2(2):12–16, July 1981.

50. Fuchs, D.: Device independent file format. TUGboat, 3(2):14–19, October 1982.

51. Farine, D. R., Strandburg-Peshkin, A., Couzin, I. D., Berger-Wolf, T. Y., and Crofoot, M. C.: Individual variation in local interaction rules can explain emergent patterns of spatial organization in wild baboons. Proceedings of the Royal Society of London B: Biological Sciences, 284(1853), 2017.

52. Strandburg-Peshkin, A., Farine, D. R., Couzin, I. D., and Crofoot, M. C.: Shared decision-making drives collective movement in wild baboons. Science, 348(6241):1358–1361, 2015.

53. Gao, Y., Liu, Y., Zhou, L., Guo, Z., Rong, M., Liu, X., Lai, C., and Ding, X.: The effects of different wavelength uv photofunctionalization on micro-arc oxidized titanium. PLoS One, 8(7):e68086, 2013.

VITA

NAME	Hélène Della Monica
EDUCATION	
	Master of Science in Mechanical Engineering, University of Illinois at Chicago, May 2019, Chicago, Illinois, USA
	Bachelor's Degree in Mechanical Engineering, Politecnico di Torino, September 2017, Torino, Italy